

AD-A009 633

ATTITUDE DETERMINATION TECHNIQUES FOR ROCKETS WITH  
INERTIAL MEASURING SYSTEMS

Brian F. Sullivan, et al

Boston College

Prepared for:

Air Force Cambridge Research Laboratories

30 November 1974

DISTRIBUTED BY:

**NTIS**

National Technical Information Service  
U. S. DEPARTMENT OF COMMERCE

DOCUMENT CONTROL DATA - R&D		
<i>(Security classification of title, body of abstract and indexing annotation must be entered when the overall report is classified)</i>		
1. ORIGINATING ACTIVITY <i>(Corporate author)</i> SPACE DATA ANALYSIS LABORATORY Boston College Chestnut Hill, Massachusetts 02167	2a. REPORT SECURITY CLASSIFICATION UNCLASSIFIED	2b. GROUP
3. REPORT TITLE ATTITUDE DETERMINATION TECHNIQUES FOR ROCKETS WITH INERTIAL MEASURING SYSTEMS		
4. DESCRIPTIVE NOTES <i>(Type of report and inclusive dates)</i> Scientific Final 18 October 1972 - 17 October 1974		
5. AUTHOR(S) <i>(First name, middle initial, last name)</i> Brian F. Sullivan Marvin E. Stick Rene J. Marcou		
6. REPORT DATE 30 November 1974	7a. TOTAL NO. OF PAGES 68	7b. NO. OF REFS 5
8a. CONTRACT OR GRANT NO. F19628-73-C-0093	9a. ORIGINATOR'S REPORT NUMBER(S)	
b. PROJECT, TASK, WORK UNIT NOS. N/A	9b. OTHER REPORT NO(S) <i>(Any other numbers that may be assigned this report)</i>	
c. DOD ELEMENT 61102F	AFCRL-TR-75-0087	
d. DOD SUBELEMENT 681300		
10. DISTRIBUTION STATEMENT Approved for public release; distribution unlimited.		
11. SUPPLEMENTARY NOTES Tech, other	12. SPONSORING MILITARY ACTIVITY Air Force Cambridge Research Laboratories Hanscom AFB, Massachusetts 01731 Contract Monitor: R.E. McInerney/SUYA	
13. ABSTRACT The implementation of procedures used to calculate the attitude of a rocket from its transmitted gyroscopic roll, pitch, and yaw signals is discussed. The differences and the angular conversions of the output from various inertial attitude systems are presented. Also, a synopsis of the mathematical analysis used to compute attitude is presented.  In addition, analyses and data reduction techniques are developed to determine the attitude of the Ute-Tomahawk rocket A09.209-1, fired 16 April 1973 at White Sands Missile Range, New Mexico. The attitude measuring system on this vehicle consisted of a Bayshore System Lunar Sensor Model number LS-11-DR-2 and a set of triaxial Schonstadt 600 milligauss magnetometers. An attitude determination problem was created when the telemetered lunar sensor angular signal was saturated for nearly the entire flight; however, the times of the lunar readout were accurately measured. Vehicle procession and spin rates were determined from corrected magnetometer data together with the available lunar information. Using the above attitude information in conjunction with corrected magnetometer data, standard attitude determination techniques discussed in [2,3] were modified to generate lunar pitch angles.		

UNCLASSIFIED

Security Classification

14. KEY WORDS	LINK A		LINK B		LINK C	
	ROLE	WT	ROLE	WT	ROLE	WT
Rocket Attitude Gyroscopic Data Attitude Calculation Lunar Sensors Angle of Attack Axis of Precession Data Simulation Magnetometer Data Inertial Measuring Systems						

11

UNCLASSIFIED

Security Classification

## TABLE OF CONTENTS

	<u>PAGE</u>
LIST OF ILLUSTRATIONS	v
INTRODUCTION	1
Section 1 ATTITUDE DETERMINATION AND REFINEMENTS FROM GYROSCOPIC DATA	3
1.1 Mars and Midas Gyroscopic Attitude Systems	3
1.2 Attitude Control System	4
1.2.1 A.C.S. Coordinate Reference	4
1.2.2 A.C.S. Output Measurements	4
1.3 Analysis and Refinement Techniques	6
1.3.1 Analysis for Determination of Rocket Attitude	6
1.3.2 Refinement Techniques for Final Outputs	8
1.3.2.1 Fourier Series Approximation	8
1.3.2.2 Nth Degree Polynomial Approximation	8
1.3.3 Statistical Studies	9
1.3.3.1 RMS Value with Application	9
1.3.3.2 Correlation Coefficient with Application	10
1.4 Vehicle Studies	11
Section 2 ATTITUDE SYSTEM FOR A09.209-1	13
2.1 Lunar Sensor	13
2.2 Photometers	14
2.3 The Magnetometers	14
2.4 Errors in the Magnetometer Readouts	14
2.5 Permanent and Induced Magnetic Fields	15
2.5.1 Data Sample Rate and Interval Selections	17
2.5.2 Polynomial Fit	17
2.6 Magnetometer Phase Shifting	18
Section 3 ATTITUDE ANALYSIS FOR THE WELL-BEHAVED PORTION OF THE FLIGHT OF A09.209-1	20
3.1 Determination of the Elevation and Azimuth of the Rocket Axis at a Lunar Readout Time	20
3.2 Determination of the Axis of Precession	21
3.3 Generation of Attitude Data	22
3.4 Quality Checks	24
3.4.1 Generating Magnetometer and Lunar Data	24

TABLE OF CONTENTS (continued)

		<u>PAGE</u>
3.4.2	Critical Value and Second Derivative Test	25
3.5	Modification in Analysis	26
Section 4	ATTITUDE ANALYSIS FOR THE REMAINING PORTIONS OF THE FLIGHT OF A09.209-1	
4.1	Ascent Portion	28
4.2	Descent Portion	29
	APPENDIX A	50
	FIGURES	33
	REFERENCES	61
	BIBLIOGRAPHY	62
	ACKNOWLEDGMENTS	63

LIST OF ILLUSTRATIONS

<u>FIGURE</u>		<u>PAGE</u>
1.	A09.209-1 Instrument Orientation	33
2.	Coordinate System	34
3.	A.C.S. Coordinate Reference	35
4.	T.D.C. Reference	36
5.	A09.107-2 Angle of Attack	37
6.	A10.205-2 Angle of Attack	38
7.	A18.105-1 Angle of Attack	39
8.	A09.210-2 Angle of Attack	40
9.	A09.210-1 Angle of Attack	41
10.	A17.110-1 Angle of Attack	42
11.	A17.110-2 Angle of Attack	43
12.	A18.205-1 Preliminary Angle of Attack	44
13.	A18.205-1 Final Angle of Attack	45
14.	Typical Linear Correlation Strengths	46
15.	Phase Relationships	12
16.	Lunar Sensor Conversion	47
17.	Field of View of Lunar Sensor	13
18.	Magnetometer Specifications	48
19.	Magnetometer Calibration	49
20.	The Effects of the Motor on the X Magnetometer	50
21.	The Effects of the Motor on the Y Magnetometer	51
22.	The Effects of the Motor on the Z Magnetometer	52
23.	LSQMAG Flowchart	53
24.	Photometer Data	54
25.	Angle of Attack A09.209-1	55
26.	Lunar Pitch Angle A09.209-1	56
27.	Magnetic Pitch Angle	57
28.	Generated Lunar Sensor Angle	58
29.	Lunar Angular Readouts for A09.209-1	59
30.	A09.209-1 Corrected Magnetometer Data	60

## INTRODUCTION

The knowledge of the ionosphere has been greatly increased in recent years through the study of data provided from rocket-borne sensors. For certain sensors, meaningful interpretation of the instrument's output can be accomplished only when the orientation of the sensor or its transporting vehicle is known. The orientation of the sensing axis of an instrument with respect to a fixed coordinate system in space is referred to as its attitude, and from the attitude of a sensor one may determine the angle it makes with any other vector such as the rocket's velocity vector or the Earth's magnetic field vector.

The first section of this report applies the data reduction techniques described in [1] to obtain the attitude and requested angular outputs for most rockets investigated. These rockets provided gyroscopic outputs which measure the vehicle's roll, pitch, and yaw with respect to a coordinate system fixed at launch.

The analysis and data reduction techniques discussed in the remaining sections of this report were utilized to determine vehicle attitude and angles of attack of the on-board probes of the Ute-Tomahawk Rocket, A09.209-1, fired 16 April 1973 at White Sands Missile Range, New Mexico.

The attitude measuring system of this rocket consisted of a set of triaxial Schonstedt 600 milligauss magnetometers and a Bayshore System Lunar Sensor Model number LS-11-DR-2. Two magnetometers which were perpendicular to the rocket axis were in the same plane as the lunar sensor but 45° out of phase (refer to Figure 1) therefore, the readings of magnetometers had to be phase shifted so that attitude system would give simultaneous readings of Earth's magnetic field and the moon.

The lunar sensor angular output was saturated for nearly the entire flight and only functioned for a few discrete points on the descent portion of the flight, but the times of the lunar readouts were determined accurately. To calculate the angle between the rocket axis and the lunar vector, techniques not included in a normal reduction of rocket attitude data were used with acceptable results. The approach undertaken incorporated modifications of existing methods with additional criterion studies [2][3]. The primary data needed was reliable magnetometer data,

both longitudinal and lateral from which the approximate angular velocity of precession and spin rate could be determined, and available lunar information. The above approach assumed the rocket to be well-behaved for some portion of the flight.

The basic coordinate system used in this report is a true north, east, and vertical cartesian coordinate system where  $\hat{e}_{\phi_c}$ ,  $\hat{e}_{\theta_c}$ ,  $\hat{e}_{r_c}$  is a system of orthonormal vectors with  $\hat{e}_{\theta_c}$  tangent to the meridian circle through the launching tower and pointing to true north,  $\hat{e}_{\phi_c}$  tangent to the circle of latitude through the launching tower and pointing east of north, and  $\hat{e}_{r_c}$  be determined by

$$\hat{e}_{r_c} = \hat{e}_{\phi_c} \times \hat{e}_{\theta_c}.$$

This system will be referred to in this report as the north, east, and vertical system (refer to Figure 2).

## SECTION 1

### ATTITUDE DETERMINATION AND REFINEMENTS FROM GYROSCOPIC DATA

#### 1.1 MARS AND MIDAS GYROSCOPIC ATTITUDE SYSTEMS

The Whittaker Corporation's Miniature Attitude Reference System (MARS) and Space Vector Corporation's Miniature Inertial Digital Attitude System (MIDAS) both provide gyroscopic outputs for the determination of rocket attitude. Both systems reference roll, pitch and yaw motion in the same manner; i.e., the roll axis coincides with the rocket axis at launch and the orientation of a gyro reference notch determines the location of the yaw axis. The pitch axis is fixed as the cross product of the yaw axis with the roll axis.

Although the gyro notch is normally set in the vertical plane containing the rocket axis at launch, it may be rotated to any orientation perpendicular to the rocket axis. Since the accuracy of the yaw and pitch depends upon the orientation of the notch [1], it is essential that its exact position be known.

Both the MARS and MIDAS systems employ a roll-stabilized platform, using two two-degrees-of-freedom gyroscopes. The gyros are supported by gimbals arranged on the platform so that the gimbals are free to rotate about the roll, pitch and yaw axes. Initially, the orientation of the platform is fixed at launch. When the vehicular motion begins to change the orientation of the platform, precession of the gyroscopes is detected by pickoffs on the corresponding output axes. Signals transmitted to a SERVO-mechanism then activate a motor which restores the platform to its initial attitude. Thus, the stabilized platform retains its orientation in inertial space, providing a fixed coordinate reference system for roll, pitch and yaw measurements.

The outputs from the MARS and MIDAS system differ considerably, and consequently different techniques are used to recover angular roll, pitch and yaw. The MARS system employs potentiometers to convert roll, pitch and yaw displacements to analog voltages, having a range of approximately 0-5 volts. Each 5-volt span represents some degree segment having a predetermined length. A sudden change in the voltage

(from 5 to 0 volts or from 0 to 5 volts) is called a swap, and it is only through the location of swaps that the correct degree span can be determined from the MARS data [1].

For a vehicle equipped with the MIDAS system, the roll, pitch and yaw measurements are digitized by means of optical encoders. As a result the one-to-one correspondence between angular displacements and digital codings satisfies

$$\phi = \frac{n}{1024} \cdot 360$$

where

$\phi$  is the angular displacement in degrees,

n is the digital coding

and 1024 counts represent 360 degrees. No bias voltages are needed for conversion as with the MARS system since the MIDAS encoders automatically represent the displacement from the uncaged position of the gyro which fixes the coordinate reference system.

## 1.2 Attitude Control System

For the Space Vector Attitude Control System (ACS), the orientation of the gyro notch is not used as a reference. Instead, the orientation of the "Top Dead Center" (TDC) supercedes all other references, and all side probe measurements are based upon the TDC position.

### 1.2.1 ACS Coordinate Reference

The ACS coordinate reference is displayed in Figure 3. The yaw, pitch and roll references duplicate those for the MARS and MIDAS systems except that gyro notch position is not available. The TDC reference as used for the ACS system is displayed in Figure 4.

### 1.2.2 ACS Output Measurements

Three models for the ACS were encountered in attitude determination - #10370, #10380, #10390. However, for data reduction, models 10370 and 10380 were treated alike. Model 10370 (10380) output roll voltage, pitch course and fine voltage, yaw course and fine voltage.

Model 10390 output only roll voltage-pitch coarse and yaw coarse voltage. The conversion to angular measurements was made with calibration curves which provided the magnitude of the angle.

The following Table 1 summarizes the ranges of the typical calibration curves for the various models. It should be noted however, that linear interpolation was not possible with all conversions.

	MODEL					
	10370		10380		10390	
	VOLTS	DEGREES	VOLTS	DEGREES	VOLTS	DEGREES
Pitch Coarse	(.54,4.36)	0 + 80	(.53,4.33)	0 + 80	(-.05,4.64)	0 + 80
Yaw Coarse	(1.37,3.56)	0 + 45	(1.37,3.56)	0 + 45	(.95, 4.14)	0 + 50
Roll	(0, 4.63)	0 + 170	(0, 4.62)	0 + 170	(0, 5)	0 + 45
Pitch Fine	(-.54,4.63)	0 + 8	(-.53,4.78)	0 + 7	-	-
Yaw Fine	(-.52,4.94)	0 + 7	(-.51,4.85)	0 + 7	-	-

TABLE 1

The sign reference for outputs can be determined from Figure 3 along with the following Table 2.

	MODEL					
	10370 & 10380			10390		
	ROLL CW	PITCH DOWN	YAW RIGHT	ROLL CW	PITCH DOWN	YAW RIGHT
Pitch Coarse	-	decreasing	-	-	decreasing	-
Yaw Coarse	-	-	increasing	-	-	increasing
Roll	increasing	-	-	decreasing	-	-
Pitch Fine	-	increasing	-	-	-	-
Yaw Fine	-	-	decreasing	-	-	-

TABLE 2

### 1.3 Analysis and Refinement Techniques

The development of analyses to calculate the attitude of a rocket from gyroscopic roll, pitch and yaw data are discussed in the following subsections. Since telemetered data may possess inherent noise, data filtering and smoothing may be required to provide continuous output. To substantiate the curve fitted data in the smoothing process, statistical studies are made to compare measured and predicted data discrepancies.

#### 1.3.1 Analysis for Determination of Rocket Attitude

According to [1], the longitudinal axis of the vehicle can be expressed as the vector  $e''_r$ :

$$e''_r = \hat{X} \cos y \cos p + \hat{Y} \sin y + \hat{Z} \cos y \sin p$$

where  $y$  and  $p$  are the yaw and pitch respectively and the body axes  $\hat{X}$ ,  $\hat{Y}$ ,  $\hat{Z}$  are in the direction of the gyro roll, pitch and yaw axes.

Given the elevation  $\theta$  and azimuth  $\phi$  of  $e''_r$  in the local North, East and Vertical system  $\hat{e}_{\theta_c}$ ,  $\hat{e}_{\phi_c}$ ,  $\hat{e}_{r_c}$  at launch, the unit vectors  $\hat{X}$ ,  $\hat{Y}$ ,  $\hat{Z}$  can be expressed as linear combinations of the earth-based-system  $\hat{e}_{\theta_c}$ ,  $\hat{e}_{\phi_c}$ ,  $\hat{e}_{r_c}$  so that we have

$$\begin{pmatrix} \hat{X} \\ \hat{Y} \\ \hat{Z} \end{pmatrix} = \begin{pmatrix} a_{11} & a_{12} & a_{13} \\ a_{21} & a_{22} & a_{23} \\ a_{31} & a_{32} & a_{33} \end{pmatrix} \begin{pmatrix} \hat{e}_{\theta_c} \\ \hat{e}_{\phi_c} \\ \hat{e}_{r_c} \end{pmatrix}$$

where the  $a_{ij}$  terms ( $i, j = 1, 2, 3$ ) are the initial direction coefficients of the gyro axes at launch.

According to equation (5) of reference [1], we can define a system of orthonormal vectors  $e''_r$ ,  $e''_1$ ,  $e''_2$  at any time in flight as a linear combination of the  $\hat{X}$ ,  $\hat{Y}$ ,  $\hat{Z}$  axes. The elevation  $\theta$  and azimuth  $\phi$  of the rocket axis or any vector perpendicular to the rocket axis can now be determined by (9) and (10) described in reference [1].

For side probe data, the orientation of the probe must be defined in the  $e_r''$ ,  $e_1''$ ,  $e_2''$  system; i.e., for  $\hat{P}$  in the direction of the probe

$$\hat{P} = e_r'' \cos\lambda + e_1'' \cos\mu \sin\lambda + e_2'' \sin\mu \sin\lambda$$

where  $\lambda$  is the angle between  $e_r''$  and  $\hat{P}$ ,  $\mu$  is the angle between  $e_1''$  and the projection of  $\hat{P}$  in the plane of  $e_1''$  and  $e_2''$ .

Since  $e_r''$ ,  $e_1''$ ,  $e_2''$  can already be expressed in the local  $\hat{e}_{\theta_c}$ ,  $\hat{e}_{\phi_c}$ ,  $\hat{e}_{r_c}$  system, only a rotation matrix involving  $\lambda$  and  $\mu$  is necessary to express  $\hat{P}$  as

$$\hat{P} = \hat{e}_{\theta_c} \cos\theta_p \cos\phi_p + \hat{e}_{\phi_c} \cos\theta_p \sin\phi_p + \hat{e}_{r_c} \sin\theta_p.$$

The angle  $\theta_p$ , measured positive up, is the elevation of the probe axis above the horizontal plane of  $\hat{e}_{\theta_c}$  and  $\hat{e}_{\phi_c}$ , and  $\phi_p$  is the azimuth of the probe axis measured from true North positive east. Throughout the remainder of this report, all such angles  $\theta$  and  $\phi$  describing the orientation of a probe or sensor axis in the local  $\hat{e}_{\theta_c}$ ,  $\hat{e}_{\phi_c}$ ,  $\hat{e}_{r_c}$  system will reference elevation and azimuth respectively.

Once the components of  $\hat{P}$  in the above system are determined and the components of the unit vector in the direction of the rocket flight are given by

$$\hat{V} = \hat{e}_{\theta_c} v_1 + \hat{e}_{\phi_c} v_2 + \hat{e}_{r_c} v_3$$

then the attack angle  $\psi$  between  $\hat{P}$  and  $\hat{V}$  is found from

$$\psi = \cos^{-1}(v_1 \cos\theta_p \cos\phi_p + v_2 \cos\theta_p \sin\phi_p + v_3 \sin\theta_p).$$

Refer to Figures (5 - 11) for typical angles of attack.

### 1.3.2 Refinement Techniques for Final Outputs

Due to noise or in-flight calibrations often times present in the recorded data, filtering procedures are modified or developed as required to provide continuous final output for the attitude determination system. The primary routines used are Fourier Series and nth degree polynomial approximations.

Typical examples of the above recorded data problems are encountered in the conversion of the ACS coarse (and fine when available) yaw and pitch data (see Section 1.2.2) to angular measurements. The random noise discontinuities in these converted outputs cause the attitude determination results to be unusable in the analysis of probe data requiring continuity of vehicle motion (refer to Figures 12 and 13).

#### 1.3.2.1 Fourier Series Approximation

To provide smooth, continuous and acceptable attitude information during the well-behaved areas of a particular vehicular flight, the coarse (and/or fine when applicable) yaw and pitch data can be predicted by the Fourier Series

$$Y = \frac{a_0}{2} + \sum_{n=1}^{\infty} (a_n \cos \frac{n\pi x}{L} + b_n \sin \frac{n\pi x}{L}) \quad (1.3-1)$$

This approach is used due to the periodic nature of the data.

For most rocket flights, quick convergence for (1.3-1) is obtained with the approximation

$$Y = A + Bt + C \sin \omega t + D \cos \omega t. \quad (1.3-2)$$

The addition of the linear term to the 1st three terms of (1.3-1) is needed to account for an occasional linear shift in the converted data. A preliminary rotation rate or angular velocity  $\omega$  is selected from a study of the oscillograms of the raw data, and is further refined by an option within the fitting routine.

#### 1.3.2.2 Nth Degree Polynomial Approximation

During regions in which a vehicle was not well-behaved, yaw and pitch outputs are separated into discrete time intervals. These intervals are then curve fitted with polynomials up to the 20th degree when necessary. The nth degree polynomial routine selects the best fit for the data calculating an RMS value (see Section 1.3.3) between

measured data and data calculated from each of the polynomial approximations. The minimum RMS value determines the best fit in the specified interval. These techniques were applied with acceptable results to A17.110-1 during regions of ascent and descent with the vehicle was not well-behaved.

### 1.3.3 Statistical Studies

For each of the data refinement techniques discussed in Section 1.3.2, RMS values are computed for the polynomial or series approximation to the measured output. However, a small RMS value can sometimes be misleading; i.e., slight unwarranted wave patterns may be created by (1.3-2) in the predicted data whereas plots of the converted yaw and pitch data indicate a strong possibility of a linear fit to the data. In cases like described in Figure 14c, additional studies of the correlation coefficient  $\rho$  are made to check whether a linear fit or equation of the form (1.3-2) would best represent the data. Computation of the RMS value together with the correlation coefficient, when required, form an integral part of the reliability assessed to the fitting routines described in Section 1.3.2.

#### 1.3.3.1 RMS Value with Application

The RMS (root mean square) deviation of a set of N values is defined to be the square root of the mean of their squares; that is

$$\text{RMS} = \sqrt{\sum_{i=1}^N \frac{(X_i - \bar{X})^2}{N}} \quad (1.3-3)$$

where  $X_i$  is the difference between a measured and time associated predicted data value, and

$$\bar{X} = \sum_{i=1}^N \frac{X_i}{N}$$

To simplify computation, (1.3-3) can be rewritten as

$$\text{RMS} = \sqrt{\sum_{i=1}^N \frac{X_i^2}{N} - \bar{X}^2} \quad (1.3-4)$$

The RMS deviation can also be referred to as the standard deviation  $\sigma$ . For a normal distribution, a  $\pm 3\sigma$  deviation accounts for  $\approx 99.7\%$  of the measured data. Therefore, tolerance levels are set on input data to

ensure that all predicted data be within the specified  $\sigma$  deviation utilizing the results of (1.3-4).

For the vehicle A18.006-4, (1.3-2) was used to generate yaw and pitch data from 80 to 375 seconds after launch. This function took into account the sinusoidal nature of the output as well as the slight linear displacement of the data. Using a sample rate of 20 points per second with an acceptance level of  $1^\circ$  between data points as input to the software routine, output showed the unknowns in (1.3-2) to be  $\omega = \frac{2\pi}{13.7273}$  with the pitch coefficients

$$A = 6.863463 \quad B = -.0026176 \quad C = .132396 \quad D = .090675$$

and the yaw coefficients

$$A = .6111509 \quad B = .0020662 \quad C = -.030052 \quad D = .179948.$$

Generating data with the above coefficient values, the RMS values for pitch and yaw were shown to be  $0.565^\circ$  and  $0.288^\circ$  respectively.

### 1.3.3.2 Correlation Coefficient with Application

For data points  $(t_i, y_i)$ , the correlation coefficient  $\rho$  is defined as

$$\rho = \frac{N \sum_{i=1}^N t_i y_i - (\sum_{i=1}^N t_i) (\sum_{i=1}^N y_i)}{\left( \left[ N \sum_{i=1}^N t_i^2 - (\sum_{i=1}^N t_i)^2 \right] \left[ N \sum_{i=1}^N y_i^2 - (\sum_{i=1}^N y_i)^2 \right] \right)^{\frac{1}{2}}}$$

$\rho$  may take on any value between -1 and +1 inclusive; and  $\rho$  close to -1 implies a strong negative correlation whereas  $\rho$  close to +1 implies a strong positive correlation.  $\rho$  close to 0 implies a weak correlation. Several examples of the strengths of linear correlation [5] are given in Figure 14..

When displaying the pitch fine and yaw fine outputs for A18.116-1, a strong negative correlation for each was found from 100 to 350 seconds after launch. Application of (1.3-2) to converted pitch fine and yaw fine data showed  $C \approx 0$  and  $D \approx 0$  as were expected. The expression for

the predicted pitch data in degrees was

$$\text{PITCH} = -.00015545T + 7.021074, \quad 100 \leq T \leq 350$$

with a resulting RMS of  $0.06^\circ$ . This RMS value was sufficiently low to allow neglecting other possible vehicle motions. Similarly, the expression for the predicted yaw data in degrees was

$$\text{YAW} = .000217566T + .4219051, \quad 100 \leq T \leq 350$$

with a resulting RMS of  $0.05^\circ$ . Again, the RMS value was well within acceptable error limits so as to allow neglecting other possible motions.

#### 1.4 Vehicle Studies

To corroborate the initial orientations of on-board sensors, measured and attitude predicted magnetometer pitch angles are compared [1]. A software package was developed to compare the phase relationship during well-behaved areas of a vehicle's flight.

This package involves a least squares study on the magnetometer data (refer to Appendix A for detailed description). The output produced includes a table of maximum (minimum) times  $T_{\text{meas}}$ , measured data values in degrees and associated  $\Delta T_{\text{meas}}$  values for the corrected magnetometer outputs. Also included are a table of maximum (minimum) times  $T_{\text{gen}}$ , predicted data values in degrees and associated  $\Delta T_{\text{gen}}$  values for the predicted magnetometer output from the attitude data. The two-time dependent tables are merged for all consecutive time values of each array and the phase shift between the associated values are printed.

For  $T_{\text{gen}} \leq T_{\text{meas}} + \Delta T_{\text{meas}}$ , the phase shift  $\chi$  between the raw and the predicted magnetometer data is

$$\chi = \left[ \frac{T_{\text{gen}} - T_{\text{meas}}}{\Delta T_{\text{meas}}} \right] \times 360.$$

For  $0 \leq \chi \leq 180^\circ$  the predicted data is lagging or coincident with the measured magnetometer data. For  $180^\circ < \chi < 360^\circ$ , the measured data is said to lag the predicted by  $360^\circ - \chi$ . The following Figure 15 depicts the relationships just discussed:

PHASE RELATIONSHIPS

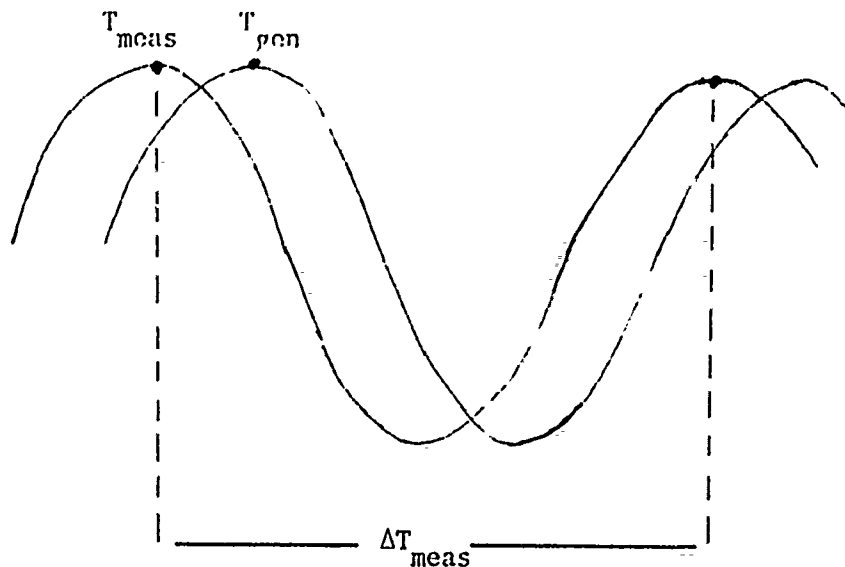


Figure 15

In this figure, the predicted data from the attitude is lagging the raw data since we are assuming that  $(T_{gen} - T_{meas}) \leq \frac{1}{2} \Delta T_{meas}$ .

## SECTION 2

### ATTITUDE SYSTEM FOR A09.209-1

The primary attitude sensing devices on board consisted of a triaxial set of magnetometers and a lunar sensor. Also aboard was a set of photometers which provided approximate lunar information. From these devices (if they function properly), it is possible to calculate the attitude for any probe at any time during the flight.

#### 2.1 Lunar Sensor

The Bayshore lunar sensor had its sensitivity set to read out a wide range of high lunar phase angles with a resolution of  $2^\circ$  and an accuracy of  $\pm 1^\circ$ . The sensor was mounted in such a way that it reads out only when the rocket axis, the moon, and the sensor axis are all in the same plane (once per spin of the rocket). The sensor output which is in the form of a digital code can be converted directly to lunar aspect angles (refer to Figure 16). The angles this sensor was capable of reading ranged from  $+70^\circ$  to  $-26^\circ$  as measured from the center line of the sensor.

FIELD OF VIEW OF LUNAR SENSOR

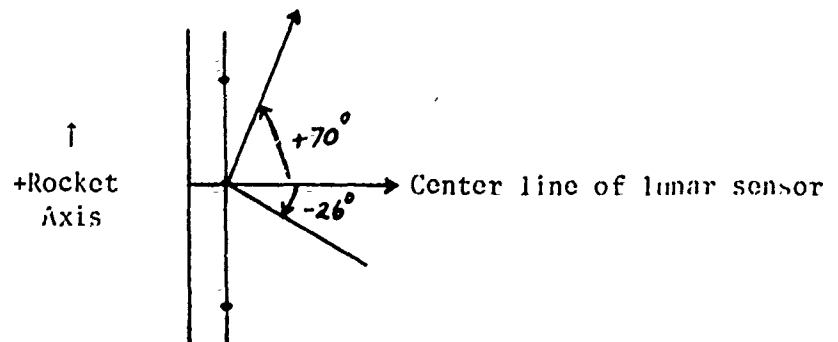


Figure 17

## 2.2 Photometers

On board this vehicle was a set of three solar blind photomultipliers with UV interference filters with a limited field of view. This set of photometers was mounted in such a manner that the projections of the three photometers on the plane perpendicular to the rocket axis were coincident with projection of the lunar sensor, i.e., the azimuth angles in the horizontal plane were equal. However, only one of the photometers was aligned with the lunar sensor and this photometer failed to function properly. The others, one with a 2750 Angstrom filter which was mounted up 5° from the horizontal plane and the other with 2600 Angstrom filter which was mounted up 10° from the horizontal plane functioned properly, (see Figure 1).

The output from these two photometers provided some important lunar information since they indicate maximum intensities when they sense the moon.

## 2.3 Magnetometers

The magnetometer system on board was a triaxial flux-gate magnetometer, specifically designed for use in rocket aspect measurement systems. A field component within the range of  $\pm 600$  milligauss is converted to an analog voltage defined by the equation of the type

$$E = 2.40 + .004 H \cos\phi$$

where  $E$  is the output in volts,  $H$  is the ambient field in milligauss and  $\phi$  is the angle between the magnetic field vector and sensor's positive magnetic axis. Figures 18 and 19 show the specifications and the vendors calibrations for this system. This calibration is done on the instrument not under simulated flight conditions.

## 2.4 Errors in Magnetometer Readouts

Since these magnetometers sense the total ambient field, the need of reliable magnetometer information requires that all permanent, stray, and induced fields should be determined as accurately as possible.

On this particular flight, there was a Siemens Brushless DC motor with four permanent magnets which spun at approximately 3,000 RPM. This motor was located 30° off the longitudinal axis and in a plane parallel to door 1, (refer to Figure 1). This motor modulated the voltage output of the three magnetometers. It created in addition to normal permanent and induced fields, two effects; first, it created a permanent magnetic field on all three axes which were modulated at the spin frequency of the motor. This effect on each axis is clearly demonstrated in Figures (20-22) where

X axis = .112 volts = 26.88 milligauss  
 Y axis = .147 volts = 35.28 milligauss  
 Z axis = .3 volts = 72 milligauss

Secondly, since the axis of the motor was not aligned parallel to a magnetometer axis, it, too, was spinning at the vehicle spin rate. This fact coupled with the absence of preflight calibration of the magnetometers under simulated flight conditions, makes orthogonality in the measurements of the magnetometers almost impossible.

## 2.5 Permanent and Induced Magnetic Fields

Since there was no preflight calibration of this set of magnetometers under flight conditions, we were unable to determine all the induced magnetic fields on each magnetometer axis. Instead, the following approach was utilized.

To minimize magnetometer output error, previously written routines\* have been implemented to correct for bias changes and induced field contributions in a mutually perpendicular three magnetometer system. Given the bias contribution parameters  $\alpha_i$ ,  $i=1,2,3$  for the X, Y and Z magnetometer outputs, respectively and the theoretical field H, we can form the equation

$$H^2 = A_1[X_{mg} + \alpha_1]^2 + A_2[Y_{mg} + \alpha_2]^2 + A_3[Z_{mg} + \alpha_3]^2.$$

$X_{mg}$ ,  $Y_{mg}$ ,  $Z_{mg}$  are the results of vendor supplied calibration curves

---

\*LSQMAG, Paul Pruneau, Space Data Analysis Laboratory, Boston College

which convert raw magnetometer output to milligauss. The least squares induced field constants,  $\sqrt{A_i}$   $i=1,2,3$  are determined by forming the sum

$$I_n = \sum [H^2 - A_1(X_{mg} + \alpha_1)^2 - A_2(Y_{mg} + \alpha_2)^2 - A_3(Z_{mg} + \alpha_3)^2]^2$$

and setting

$$\frac{\partial I_n}{\partial A_i} = 0 \quad i=1,2,3$$

This will form a system of three equations with three unknowns and a unique solution can be found for the  $A_i$  constants so long as the determinant of the coefficients does not vanish.

The software package iterates upon the  $\alpha_i$  values for a given iteration interval and determines the  $A_i$  constants for each iteration. An RMS (Root Mean Square) is then computed between the measured total magnetic field and the theoretical total field. Those values of  $\alpha_i$  and associated  $\sqrt{A_i}$  values,  $i=1,2,3$  for which the RMS is a minimum are the permanent and induced field corrections to the magnetometer output. A flow chart of the logic contained in this routine as displayed in Figure 23. This method gives the best average inducing effect on each axis, but it does not give a true representation of the induced fields.

A true representation of the outputs, where the actual magnetic field on each magnetometer axis was known, would be given by the system

$$\begin{aligned} X'_m &= X_t + b_1 X_t + b_2 Y_t + b_3 Z_t + X_{perm} \\ Y'_m &= Y_t + b_4 X_t + b_5 Y_t + b_6 Z_t + Y_{perm} \\ Z'_m &= Z_t + b_7 X_t + b_8 Y_t + b_9 Z_t + Z_{perm} \end{aligned} \quad (2.5-1)$$

where

$X'_m, Y'_m, Z'_m$  are the actual magnetometer outputs containing all types of magnetic influence

$X_t, Y_t, Z_t$  are the true magnetic fields that the magnetometers should be reading

$X_{perm}, Y_{perm}, Z_{perm}$  are the permanent fields on each axis

$b_1 - b_9$  are the induced fields

Since accurate permanent fields (bias) were needed for later analysis, additional studies were performed as outlined below.

### 2.5.1 Data Sample Rate and Interval Section

In order to accurately determine the times of maximum magnetometer output (see Appendix A), smooth magnetometer readings are required. Normal data transmission does not provide such smooth output, so to allow for proper usage of the routines described in Appendix A, a curve fit was put through the bias values of the magnetometer data. The samples selected for this fit were taken from the well-behaved portion of flight - i.e., from approximately 40 kms. on ascent to approximately 40 kms. on descent. Since the rotation rate of the magnetometer output was  $\approx .175$  seconds and every other point of the available 333 samples per second for each magnetometer was used, we had available 166 points per second or 29 points per rotation.

Three 120 second time intervals [65,185), [185,305), and [305,425) were used to obtain a separate bias approximation B for each interval from the equation

$$\sum (V_i - B) = 0$$

where  $V_i$  represents the data sample. This equation reduces to

$$B = \frac{\sum V_i}{n} .$$

In the 120 second time interval, a simple calculation shows that the number of data points n is 20,000.

### 2.5.2 Polynomial Fit

The standard bias equation as a function of time is approximated by a first degree polynomial. However to obtain greater accuracy with higher order terms in the fitting routine results, the value of the bias B(t) as a function of time t was equated with a 2nd degree polynomial to give

$$B(t) = at^2 + bt + c.$$

However, from the discussion above we can approximate B(t) by  $\frac{\sum V_i}{n}$

in each of the intervals studied. This, in turn, leads to the system of equations

$$at_1^2 + bt_1 + c = B_1$$

$$at_2^2 + bt_2 + c = B_2$$

$$at_3^2 + bt_3 + c = B_3$$

where  $t_j$ ,  $j=1,2,3$  is taken as the mean time in the  $j$ th interval and

$$B_j = \frac{\sum_{i=1}^n V_i}{n} \quad j=1,2,3$$

As the value of  $n$  increases, the maximum error that occurs in the approximation of  $B_j$  decreases. This fact can be verified by

calculations on the expression  $\frac{\sum V_i}{n}$ .

This procedure to determine the bias equation as a function of time, forms part of the procedure used on all vehicle flights when examining phase shifts between measured and predicted data.

## 2.6 Magnetometer Phase Shifting

To properly utilize the attitude determination technique mentioned in [2][3] it is necessary to have simultaneous readings of the Earth's magnetic field and the moon from attitude sensing devices with the same orientation on the vehicle. On this particular vehicle, both the lunar sensor and both the lateral magnetometers were mounted normal to the axis of the rocket, but they were out of phase by  $45^\circ$  (refer to Figure 1).

To properly align a magnetometer axis parallel to the lunar sensor axis, we begin by defining the unit vectors  $\hat{Y}$  and  $\hat{Z}$  along the Y and Z magnetometers axes respectively as

$$\hat{Y} = \hat{e}_{\theta_c} \cos\theta_y \cos\phi_y + \hat{e}_{\phi_c} \cos\theta_y \sin\phi_y + \hat{e}_{r_c} \sin\theta_y$$

$$\hat{Z} = \hat{e}_{\theta_c} \cos\theta_z \cos\phi_z + \hat{e}_{\phi_c} \cos\theta_z \sin\phi_z + \hat{e}_{r_c} \sin\theta_z.$$

Then the unit vector,  $\hat{U}$ , along the lunar sensor axis and in the plane of  $\hat{Y}$  and  $\hat{Z}$ , can be expressed as

$$\hat{U} = \hat{Y} \cos \chi + \hat{Z} \sin \chi$$

where  $\chi$  is the angle between the lunar sensor axis and Y magnetometer axis.

Then the scalar product of the Earth's unit magnetic field vector  $H$  with  $\hat{U}$  where

$$H = \hat{e}_{\theta_c} x_m + \hat{e}_{\phi_c} y_m + \hat{e}_{r_c} z_m$$

is given by

$$\cos \gamma = (H \cdot \hat{U}) = (H \cdot \hat{Y}) \cos \chi + (H \cdot \hat{Z}) \sin \chi$$

where  $(H \cdot \hat{Y})$  and  $(H \cdot \hat{Z})$  are equal to the actual normalized magnetometer outputs  $H_y$  and  $H_z$ .

Then

$$H_u = \cos \gamma = H_y \cos \chi + H_z \sin \chi$$

is the expression that represents the cosine of the angle between the magnetic field and the lunar sensor axis.

Accurate knowledge of the bias of this generated magnetometer data (or the times when this magnetometer is reading approximately zero magnetic field) is helpful in the attitude analysis. Therefore, the numerical methods previously discussed in sections (2.5.1) and (2.5.2) were applied to this data.

## SECTION 3

### ATTITUDE ANALYSIS FOR THE WELL-BEHAVED PORTION OF THE FLIGHT

The basic attitude determination analysis for this vehicle uses a combination of available lunar information and corrected magnetometer data. The available lunar information was obtained through interpretation of the behavioral pattern of the photometer data at selected times, through the accurate times of the lunar sensor readout (even though the sensor angular output was saturated for the most of the flight), and through techniques which allow the lunar angle to be determined when specified criteria are fulfilled.

#### 3.1 Determination of the Elevation and Azimuth of the Rocket Axis at a Lunar Readout Time

Let  $\hat{X}$ ,  $\hat{U}$ ,  $\hat{W}$  be a orthonormal system with  $\hat{X}$ , a unit vector in direction of the rocket axis,  $\hat{U}$ , a unit vector perpendicular to the rocket axis at the lunar sensor, and  $\hat{X} \times \hat{U} = \hat{W}$ . Since we know the lunar sensor reads out only when the moon is in the plane of  $\hat{X}$  and  $\hat{U}$ ,

$$M = M_x \hat{X} + M_u \hat{U} \quad (3.1-1)$$

and representing the magnetic field in this vehicle system

$$H = H_x \hat{X} + H_u \hat{U} + H_w \hat{W}. \quad (3.1-2)$$

In (3.1-1) and (3.1-2) as well as in the following discussions,  $M$  and  $H$  are assumed to be unit vectors. The scalar product of the vectors  $H$  and  $M$  is then given by

$$(H \cdot M)_1 = H_x M_x + M_u H_u. \quad (3.1-3)$$

The scalar product can also be derived from empirical sources where

$$M = \hat{e}_{\theta_c} m_1 + \hat{e}_{\phi_c} m_2 + \hat{e}_{r_c} m_3 \quad (3.1-4)$$

and

$$H = \hat{e}_{\theta_c} x_m + \hat{e}_{\phi_c} y_m + \hat{e}_{r_c} z_m. \quad (3.1-5)$$

Then

$$(H \cdot M)_2 = m_1 x_m + m_2 y_m + m_3 z_m. \quad (3.1-6)$$

From (3.1-3) and (3.1-6)

$$(H \cdot M)_2 = H_x M_x + M_u H_u \quad (3.1-7)$$

and if the magnetometer parallel to the axis reads a zero magnetic field (refer to section 2.6) at the time of a lunar sensor readout then from (3.1-7), it is possible to determine an angular output from the lunar sensor since

$$M_x = \frac{(H \cdot M)_2}{H_x}$$

and

$$M_u = \sin(\cos^{-1}(M_x)).$$

The elevation  $\theta_x$  and the azimuth  $\phi_x$ , of the rocket axis from the equations on page 8 of [3].

$$\sin \theta_x = \frac{(H_x - (H \cdot M)M_x)z_m + (M_x - (H \cdot M)H_x)m_3 + (HM_x)(y_m m_1 - m_2 x_m)}{1 - (H \cdot M)^2} \quad (3.1-8)$$

$$\tan \phi_x = \frac{(H_x - (H \cdot M)M_x)y_m + (M_x - (H \cdot M)H_x)m_2 + (HM_x)(x_m m_3 - z_m m_1)}{(H_x - (H \cdot M)M_x)x_m + (M_x - (H \cdot M)H_x)m_1 + (HM_x)(z_m m_2 - m_3 y_m)} \quad (3.1-9)$$

where from (3.1-1) and (3.1-2)

$$(HM_x) = -H_w M_u.$$

### 3.2 Determination of the Axis of Precession

After an orientation of the rocket axis during the well-behaved portion of the flight has been determined, the equations in [2] page 15, were applied to determine the axis of precession.

Then  $\theta_p$ , the elevation of the axis of precession, and  $\phi_p$ , the

azimuth are given by

$$\theta_p = \sin^{-1} \left\{ \frac{(\cos\beta_H - \cos\gamma_1 \cos\alpha) z_m + (\cos\alpha - \cos\gamma_1 \cos\beta_H) \sin\theta_x + (He_N e_r) (He_N \hat{e}_{r_c})}{\sin\gamma_1^2} \right\} \quad (3.2-1)$$

$$\phi_p = \tan^{-1} \left\{ \frac{(\cos\beta_H - \cos\gamma_1 \cos\alpha) y_m + (\cos\alpha - \cos\gamma_1 \cos\beta_H) \cos\theta_x \sin\phi_x + (He_N e_r) (He_N \hat{e}_{\phi_c})}{(\cos\beta_H - \cos\gamma_1 \cos\alpha) x_m + (\cos\alpha - \cos\gamma_1 \cos\beta_H) \cos\theta_x \cos\phi_x + (He_N e_r) (He_N \hat{e}_{\theta_c})} \right\} \quad (3.2-2)$$

where

$e_N$  - an orientation of the rocket axis X is given by

$$\hat{e}_\theta \cos\theta_x \cos\phi_x + \hat{e}_{\phi_c} \cos\theta_x \sin\phi_x + \hat{e}_{r_c} \sin\theta_x$$

$e_r$  = the axis of precession

$$= \hat{e}_\theta \cos\theta_p \cos\phi_p + \hat{e}_{\phi_c} \cos\theta_p \sin\phi_p + \hat{e}_{r_c} \sin\theta_p$$

$$\cos\gamma_1 = (H \cdot e_N)$$

$$\cos\alpha = \frac{1}{2} \text{ cone angle} = (e_N \cdot e_r)$$

$$\cos\beta_H = \text{the angle the magnetic field vector makes with axis of precession} = (H \cdot e_r)$$

$$(He_N e_r) = \pm \sqrt{\sin^2\alpha \sin^2\beta_H - (\cos\gamma_1 - \cos\beta_H \cos\alpha)^2}$$

$$(He_N \hat{e}_{r_c}) = y_m \cos\theta_x \cos\phi_x - x_m \cos\theta_x \sin\phi_x$$

$$(He_N \hat{e}_{\phi_c}) = x_m \sin\theta_x - z_m \cos\theta_x \cos\phi_x$$

$$(He_N \hat{e}_{\theta_c}) = z_m \cos\theta_x \sin\phi_x - y_m \sin\theta_x$$

### 3.3 Generation of Attitude Data

Once the axis of precession is determined, then the generating equation for the rocket axis X which is represented by  $e_r''$  at any time t, is given by a slight modification of equation 2 page 4 of [4].

$$e_r'' = e_r \cos\alpha + e_\theta \sin\alpha \cos(\omega_0 t + \chi) + e_{\phi_c} \sin\alpha (\sin\omega_0 t + \chi) \quad (3.3-1)$$

where

$$e_{\theta} = \frac{\partial e_r}{\partial \theta} = -\hat{e}_{\theta_c} \sin \theta_p \cos \phi_p - \hat{e}_{\phi_c} \sin \theta_p \sin \phi_p + \hat{e}_{r_c} \cos \theta_p$$

$$e_{\phi} = \frac{1}{\cos \theta_p} \frac{\partial e_r}{\partial \phi} = -\hat{e}_{\theta_c} \sin \phi_p + \hat{e}_{\phi_c} \cos \phi_p$$

$$\chi = \tan^{-1} \frac{(H \cdot e_{\theta})}{(H \cdot e_{\phi})} - \omega_0 t_0 \text{ at a time, } t_0, \text{ of the maximum of axial magnetometer}$$

Transforming  $e_r''$  to the North, East, and vertical system, let

$$\begin{aligned} a_{11} &= e_r \cdot \hat{e}_{\theta_c} & a_{12} &= e_r \cdot \hat{e}_{\phi_c} & a_{13} &= e_r \cdot \hat{e}_{r_c} \\ a_{21} &= e_{\theta} \cdot \hat{e}_{\theta_c} & a_{22} &= e_{\theta} \cdot \hat{e}_{\phi_c} & a_{23} &= e_{\theta} \cdot \hat{e}_{r_c} \\ a_{31} &= e_{\phi} \cdot \hat{e}_{\theta_c} & a_{32} &= e_{\phi} \cdot \hat{e}_{\phi_c} & a_{33} &= e_{\phi} \cdot \hat{e}_{r_c} \end{aligned}$$

then

$$\begin{aligned} e_r'' &= \hat{e}_{\theta_c} (a_{11} \cos \alpha + a_{21} \sin \alpha \cos (\omega_0 t + \chi) + a_{31} \sin \alpha \sin (\omega_0 t + \chi)) \\ &+ \hat{e}_{\phi_c} (a_{12} \cos \alpha + a_{22} \sin \alpha \cos (\omega_0 t + \chi) + a_{32} \sin \alpha \sin (\omega_0 t + \chi)) \quad (3.3-2) \\ &+ \hat{e}_{r_c} (a_{13} \cos \alpha + a_{23} \sin \alpha \cos (\omega_0 t + \chi)) \end{aligned}$$

and expressing (3.3-2) in terms of direction cosines

$$e_r'' = \hat{e}_{\theta_c} \cos \alpha_{\theta} + \hat{e}_{\phi_c} \cos \alpha_{\phi} + \hat{e}_{r_c} \cos \alpha_r \quad (3.3-3)$$

where

$$\cos \alpha_{\theta} = e_r'' \cdot \hat{e}_{\theta_c}$$

$$\cos \alpha_{\phi} = e_r'' \cdot \hat{e}_{\phi_c}$$

$$\cos \alpha_r = e_r'' \cdot \hat{e}_{r_c}$$

$e_r''$  can also be expressed in terms of its elevation  $\theta_a$  and azimuth,  $\phi_a$  angles by

$$e_r'' = \hat{e}_{\theta_c} \cos\theta_a \cos\phi_a + \hat{e}_{\phi_c} \cos\theta_a \sin\phi_a + \hat{e}_{r_c} \sin\theta_a. \quad (3.3-4)$$

Then by equating coefficients of (3.3-3) with (3.3-4), the attitude at any time,  $t$  is given by

$$\begin{aligned} \sin\theta_a &= \cos\alpha_r \\ \theta_a &= \sin^{-1}(\cos\alpha_r) \\ \tan\phi_a &= \frac{\cos\alpha_\phi}{\cos\alpha_\theta} \\ \phi_a &= \tan^{-1}\left(\frac{\cos\alpha_\phi}{\cos\alpha_\theta}\right). \end{aligned}$$

### 3.4 Quality Checks

To properly check for the best determination of the axis of precession, we proceeded in the following manner. First, the angles between the rocket axis and the Earth's magnetic field vector and the moon were generated. Then the times of the minimums and the maximums of the generated data were found and the comparison of these times with the ones from the actual data were made by the use of the techniques described in Section 1.4. The axis of precession which generated data best meeting the experimenter's criteria, together with the best comparison between the actual and the generated outputs was selected.

#### 3.4.1 Generating Magnetometer and Lunar Data

The simulation of the angles of the rocket axis makes with the Earth's magnetic field and the moon was performed by taking scalar products of equation (3.3-3) with (3.1-4) and (3.1-5), i.e.,

$$H_r''(t) = H \cdot e_r'' = x_m \cos\alpha_\theta + y_m \cos\alpha_\phi + z_m \cos\alpha_r \quad (3.4-1)$$

and

$$M_r''(t) = M \cdot e_r'' = m_1 \cos\alpha_\theta + m_2 \cos\alpha_\phi + m_3 \cos\alpha_r \quad (3.4-2)$$

### 3.4.2 Critical Values and Second Derivation Test

Once the data is generated, the times of the maximum have to be known. First, the critical values  $H''_r(t)$  and  $M''_r(t)$  must be found. This is done by letting

$$h_r = H \cdot e_r \quad h_\theta = H \cdot e_\theta \quad h_\phi = H \cdot e_\phi.$$

Then from (3.3-1)

$$h''_r(t) = H \cdot \alpha'' = h_r \cos \alpha + h_\theta \sin \alpha \cos(\omega_0 t + \chi) + h_\phi \sin \alpha (\sin \omega_0 t + \chi) \quad (3.4.2-1)$$

and the critical values are given by

$$\frac{\partial h''_r(t)}{\partial t} = \omega_0 \sin \alpha [h_\theta - \sin(\omega_0 t + \chi) + h_\phi \cos(\omega_0 t + \chi)] = 0$$

i.e., when  $\tan(\omega_0 t + \chi) = \frac{h_\phi}{h_\theta} = \frac{-h_\phi}{h_\theta}$ .

From [4] by the second derivative test, if  $t_0$  is the time when

$$\tan(\omega_0 t_0 + \chi) = \frac{h_\phi}{h_\theta},$$

$$\cos(\omega_0 t_0 + \chi) = \frac{h_\theta}{\sqrt{h_\theta^2 + h_\phi^2}} \quad (3.4.2-2)$$

and

$$\sin(\omega_0 t_0 + \chi) = \frac{+h_\phi}{\sqrt{h_\theta^2 + h_\phi^2}}, \quad (3.4.2-3)$$

then  $t_0$  is a time of a maximum for (3.4.2-1).

Substituting (3.4.2-2) and (3.4.2-3) in (3.4.2-1), we find that

$$h''_r(t_0) = h_r \cos \alpha + \sin \alpha \sqrt{h_\theta^2 + h_\phi^2}$$

but

$$h_r = \cos \beta_H \quad \text{and} \quad \sqrt{h_r^2 + h_\theta^2 + h_\phi^2} = 1$$

implies

$$\sqrt{h_\theta^2 + h_\phi^2} = \sin \beta_H$$

then

$$\begin{aligned}h''_r(t_0) &= \cos\beta_H \cos\alpha + \sin\beta_H \sin\alpha \\ &= \cos(\beta_H - \alpha).\end{aligned}\tag{3.4.2-4}$$

Similarly, if  $t_1$  is the time when  $h''_r(t)$  is a minimum then

$$h''_r(t_1) = \cos(\beta_H + \alpha).\tag{3.4.2-5}$$

When the axis of precession is not constant, equations (3.4.2-4) and (3.4.2-5) do not hold since  $\beta_H$  and  $\alpha$  then become functions of time.

### 3.5 Modification in Analysis

Using the preceding analysis together with some realistic lunar sensor angles supplied by the experimenter, the attitude was determined for the well-behaved area. Further inspection by the experimenter of his photometer data showed that the initial lunar data originally supplied was outside the acceptable range ( $\pm 4^\circ$ ). From the structural pattern of the photometer data (Figure 24) and its location on the payload (Figure 1), it was possible to determine an approximate angle the moon makes with the lunar sensor at certain times. These determinations all reflect  $\pm 4^\circ$  of accuracy and  $\pm .5$  seconds in time due to the variations in the telemetered photometer data. The existing attitude analysis was modified as described below to arrive at the best attitude solution for this lunar information.

Let  $\{T\}$  be the set of the times of the lunar readouts and their associated magnetometer readings in one second interval of the time supplied from the photometer information. We can define  $\{T\}$  as

$$\{T\} = \{t_1, \dots, t_{pk}, \dots, t_k\}$$

where  $t_{pk}$  is the time of a lunar readout closest to the time supplied by the photometer data.

and

$$t_1 \approx t_{pk} - \frac{1}{2} \text{ second.}$$

$$t_k \approx t_{pk} + \frac{1}{2} \text{ second.}$$

Let  $\{L\}$ , be the set of lunar angles, where  $L_{pk}$  is the approximate angular value derived from the photometer data given by

$$\{L\} = L_1, \dots, L_{pk}, \dots, L_k$$

where

$$L_1 = L_{pk} - 4^\circ$$

$$L_k = L_{pk} + 4^\circ$$

Finally let  $\{TxL\}$  be the set of all combinations of set T and L taking two at a time.

$$\{TxL\} = \{(t_1, L_1), (t_1, L_2), \dots, (t_1, L_k), \dots, (t_k, L_k)\} .$$

Then the attitude was calculated for each of the points of the set  $\{TxL\}$  by equations (2.1-7), (2.1-8) and (2.1-9). An axis of precession was calculated for each of these orientations by (2.2-1) and (2.2-2) and the lunar and magnetic field information simulated by (2.4-1).

The magnetic pitch angles for the axial magnetometerer, generated by using each of the calculated axes of precession discussed above, were compared with actual magnetic pitch angle (see Section 1.4). The orientation of the axis of precession that produced a minimum RMS measure (see Section 1.3.3.1), that satisfied all the behavioral patterns of the actual magnetometer data and all the experimenter's lunar criteria, was selected.

## SECTION 4

### ATTITUDE ANALYSIS FOR REMAINING PORTION OF THE FLIGHT

For the entire time the photometers functioned properly (i.e., 51-376 seconds) continuous attitude information is needed even when the rocket's axis of precession is not constant. This requirement means the attitude had to be determined for certain ascent and descent portions of the flight for which Section 3 does not apply. The approaches to determine the attitude differed according to the nature of the attitude information available.

The final results of the technique described below in addition to those results previously described were accepted by the experimenter (see Figures (25 - 30)). A particular result of this analysis, namely, the angle between the lunar probe and the moon vector compared favorably (within  $4^\circ$ ) with lunar sensor outputs from a similar flight.

#### 4.1 Ascent Portion

For the ascent portion of the flight, there was no lunar angular information available. To determine attitude during this portion of the flight, i.e., from 51 seconds to 90.2 seconds after launch, the orientation of the rocket axis at 90.2 seconds known from the analysis for the well-behaved portion of the flight was used as a reference position from which to work backwards. The apparent precessional motion of the axial magnetometer data from 62.8 to 90.2 seconds was used together with (3.2-1) and (3.2-2) to determine an apparent axis of precession during this period. At this point, we could simulate lunar and magnetic information with respect to the rocket axis by using (3.4-1) and (3.4-2) respectively. In a similar manner, i.e., using the generated orientation of the rocket axis at 62.8 seconds and the precessional motion of the axial magnetometer data from 51 to 62.8 seconds, the attitude was determined for the rocket axis back to 51 seconds. The results in each of the intervals discussed satisfied the data requirements of the axial magnetometer plus all the behavioral characteristics of the photometer data.

#### 4.2 Descent Portion

Unlike the ascent portion, two types of lunar angular information were available. The first consisted of lunar sensor angular outputs at a few discrete points, but these angles reflect a four-degree cone of uncertainty (refer to Figure 31)). The attitude was then calculated for these points using equations (3.1-8) and (3.1-9). The other type depended upon the fact that the axial magnetometer read approximately zero magnetic field at about 360 seconds after launch. Then equation (3.1-7) now yields

$$(H \cdot M)_2 = M_u H_u .$$

Therefore

$$M_u = \frac{(H \cdot M)_2}{H_u}$$

and

$$M_x = \sin(\cos^{-1}(M_u)).$$

Thus, the attitude could be calculated at this point using equation (3.1-8) and (3.1-9).

Since continuous attitude information is required for this portion and the axis of precession was not constant, studies showed it to vary at approximately the same rate as the midpoint of the curve of the axial magnetometer output (see Figure 32)). Then using this information together with the behavioral pattern of photometer data and the discrete attitude points, the techniques discussed in Section 3 were modified to generate the attitude information. The acceptance tests for the attitude data here were the same as for the well-behaved area.

## APPENDIX A

### MAXIMUM OUTPUTS OF THE MAGNETOMETER DATA

#### A. Specification of Curve Fitted Data Areas

Given the sinusoidal nature of the lateral magnetometer outputs, the prepared software routines have the capability of determining either the times of relative maximum outputs or the times of relative minimum outputs. If a least squares approximation of the data is desired in the maximum areas of the output, then a test is performed on the data  $V_i$  satisfying the inequality

$$B(t_i) < V_i.$$

Likewise, if a fit of the minimum areas is desired, then only those  $V_i$  values satisfying the inequality

$$B(t_i) > V_i$$

are stored for computation in the least squares polynomial fits of the specified areas of the data.

#### B. Acceptance Level for the Least Squares Data

In order to initiate the procedure for storing data in the maximum areas of the least squares approximation, a value  $V_i$  must be found such that  $V_i > B(t_i)$  and  $V_{i-1} \leq B(t_{i-1})$ . Once initiated, data is stored until  $V_j < B(t_j)$  and  $V_{j-1} \geq B(t_{j-1})$  where  $j > i$ . This last condition is a necessary one for ending the sample region but not a sufficient condition. The sufficiency test is made by examining  $V_{j+1}$  to ensure that  $V_j$  is not a noise point. If  $V_{j+1} < B(t_{j+1})$  then a least squares parabolic fit is performed on the sampled data. However, if  $V_{j+1} \geq B(t_{j+1})$ , the point  $V_j$  is discarded and the summing procedure of the least squares continues. Similar tests are made in the minimum regions of fitted data except that the inequality signs are reversed.

#### C. Least Squares Approximation

##### 1. 1st derivative test.

In each specified region, the data is fit to the quadratic

$$Y = \bar{A}t^2 + \bar{B}t + \bar{C}.$$

The value of the bias  $B(t_i)$  at which the sampling begins and that value  $B(t_j)$ ,  $j > i$  at which the sampling ends are obviously just the points of inflection for the sinusoidal curve. The time of relative maximum (minimum) is obtained by setting  $\frac{dY}{dt} = 0$  and solving for time  $t$ . This, in turn, provides us with a predicted output value

$$Y = \bar{A}T_M^2 + \bar{B}T_M + \bar{C}$$

where

$$T_M = -\frac{\bar{B}}{2\bar{A}}$$

## 2. Error tolerance

Should the measured and predicted outputs deviate by more than some specified limit, usually taken to be 4%, the acceptance level for least squares data may be modified so that the sampled regions more closely approximate the parabolic fit. This modification amounts to accepting the area containing maximum data when  $V_i > B(t_i) + k$  where  $k$  is a constant determined from examination of the oscillographs. For minimum output regions, the inequality takes the form  $V_i < B(t_i) - k$ .

## 3. Output quantities

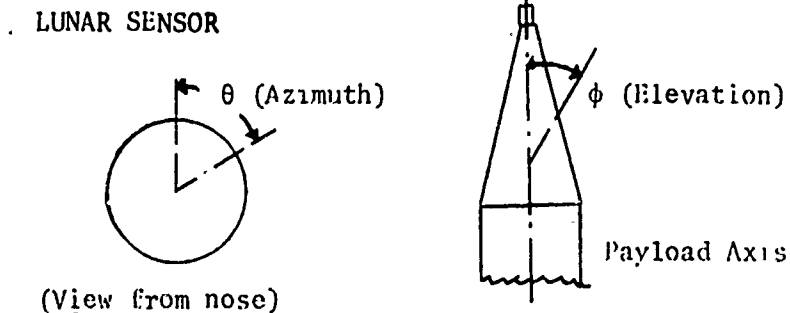
For each value of  $T_M$  generated by the 1st derivative test, an associated  $Y(T_M)$  value and  $\Delta T_M$  are output. Special note is made of any value of  $\Delta T_M$  outside a specified interval about the assumed rotation rate and further investigations of these areas are undertaken as necessary. A mean  $\Delta T_M$  value is computed for the well-behaved portion of the flight and output at the end of the data pass. This  $\Delta T_M$  value for each lateral magnetometer normally consists of spin and precessional motion and, therefore, is referred to as the rotation rate.

Although no specific mention as yet has been made of the axial magnetometer output, the routines apply equally as well in the case of this magnetometer. Computation of maximum and minimum values provide us with a good approximation to the cone angle of the vehicle axis. Should the output exhibit only the slightest variance in successive maximum and minimum values respectively, then the vehicle axis motion is due almost entirely to precessional motion and the cone angle will remain nearly constant.

If the vehicle axis study option is desired in addition to the lateral magnetometers, supplemental outputs include the cone angles and precession period of the vehicle axis.

UTE TOMAHAWK A09.209-1

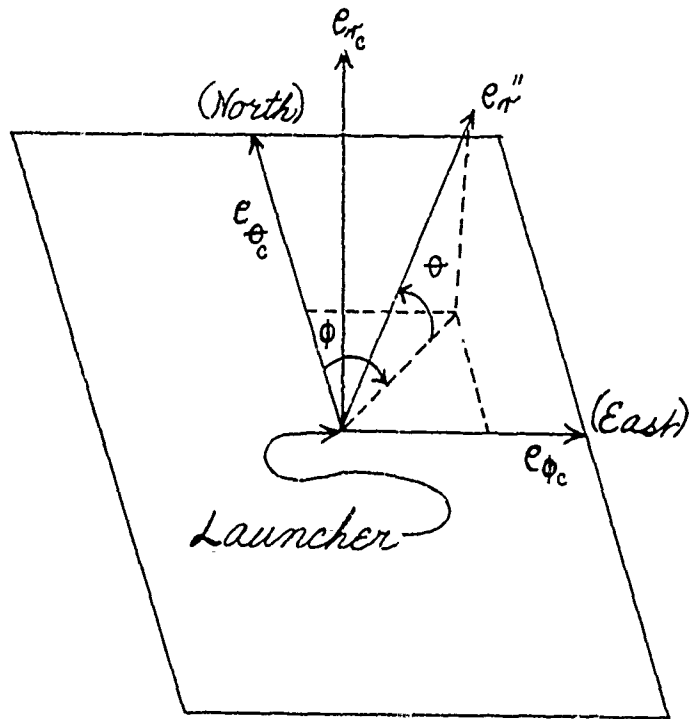
INSTRUMENT ORIENTATIONS



INSTRUMENT	AZIMUTH (degrees)	ELEVATION (degrees)
X Magnetometer	0	0
Y Magnetometer	225°	90°
Z Magnetometer	315°	90°
Lunar Sensor	0	90°
2750 A Photometer	0	85°
2600 A Photometer	0	80°
Siemens Brushless Motor	90°	30°

Figure 1

COORDINATE SYSTEM



$\theta$  = Elevation of  $e_r''$

$\phi$  = Azimuth of  $e_r''$

Figure 2

# ACS COORDINATE REFERENCE

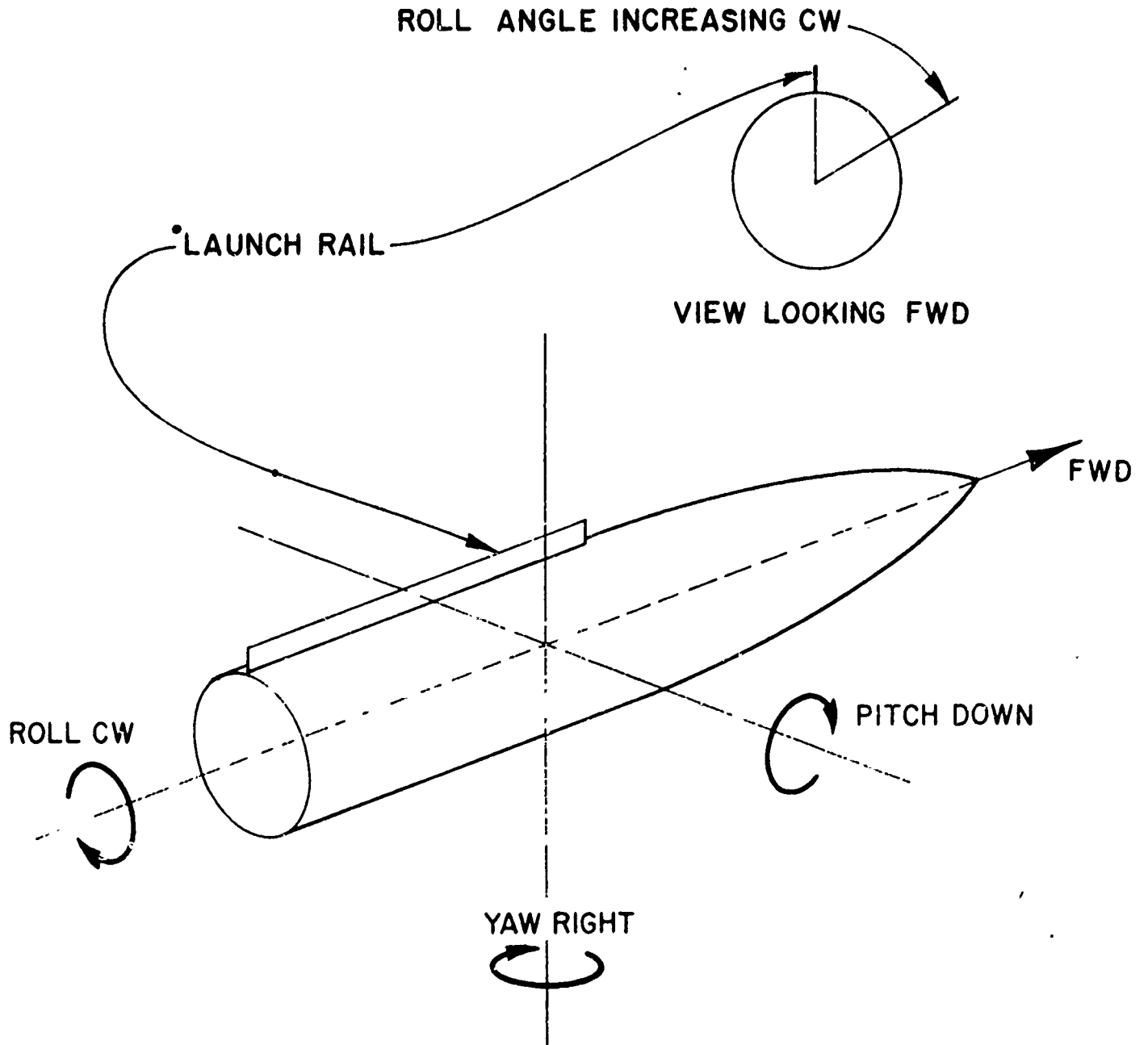


Figure 3

• LAUNCH RAIL = 0 degrees ROLL

TDC REFERENCE

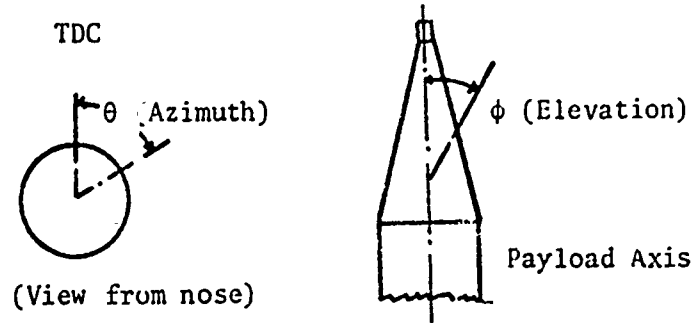


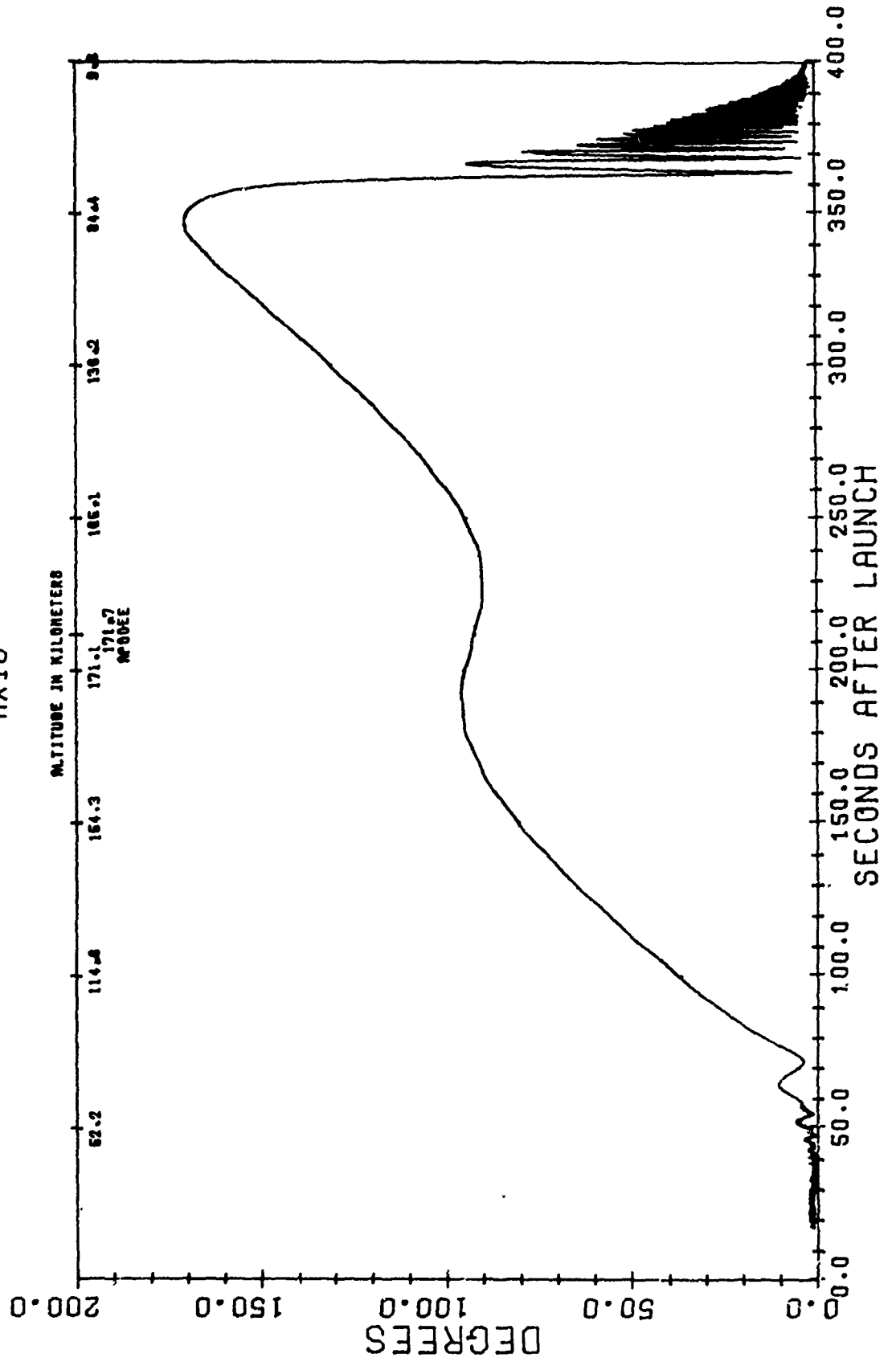
Figure 4

Figure 5

AG9.107-2

ANGLE OF ATTACK

AXIS



A10.205-2  
ANGLE OF ATTACK  
AXIS

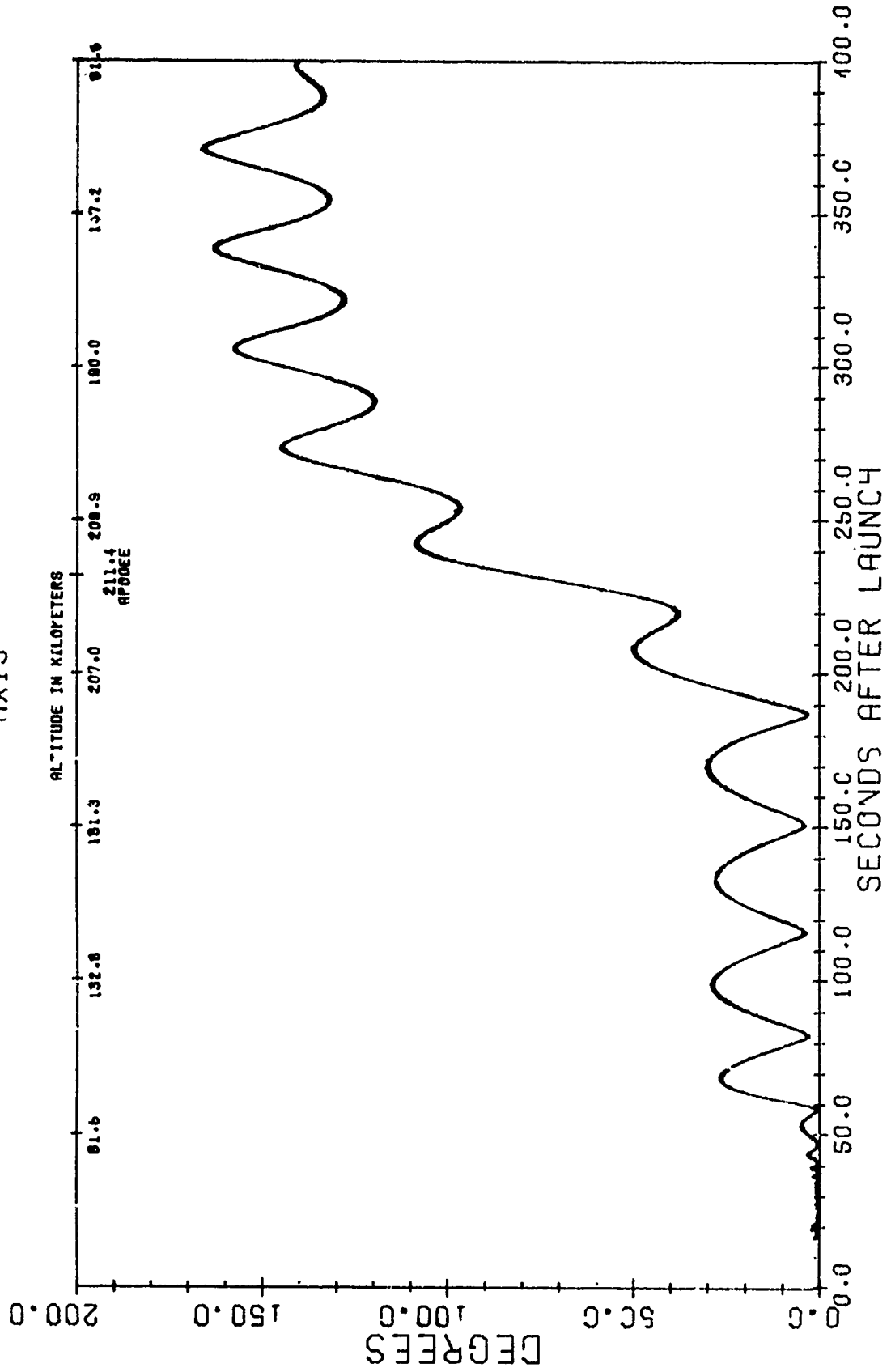


Figure 6

A18.109-1

ANGLE OF ATTACK

AXIS

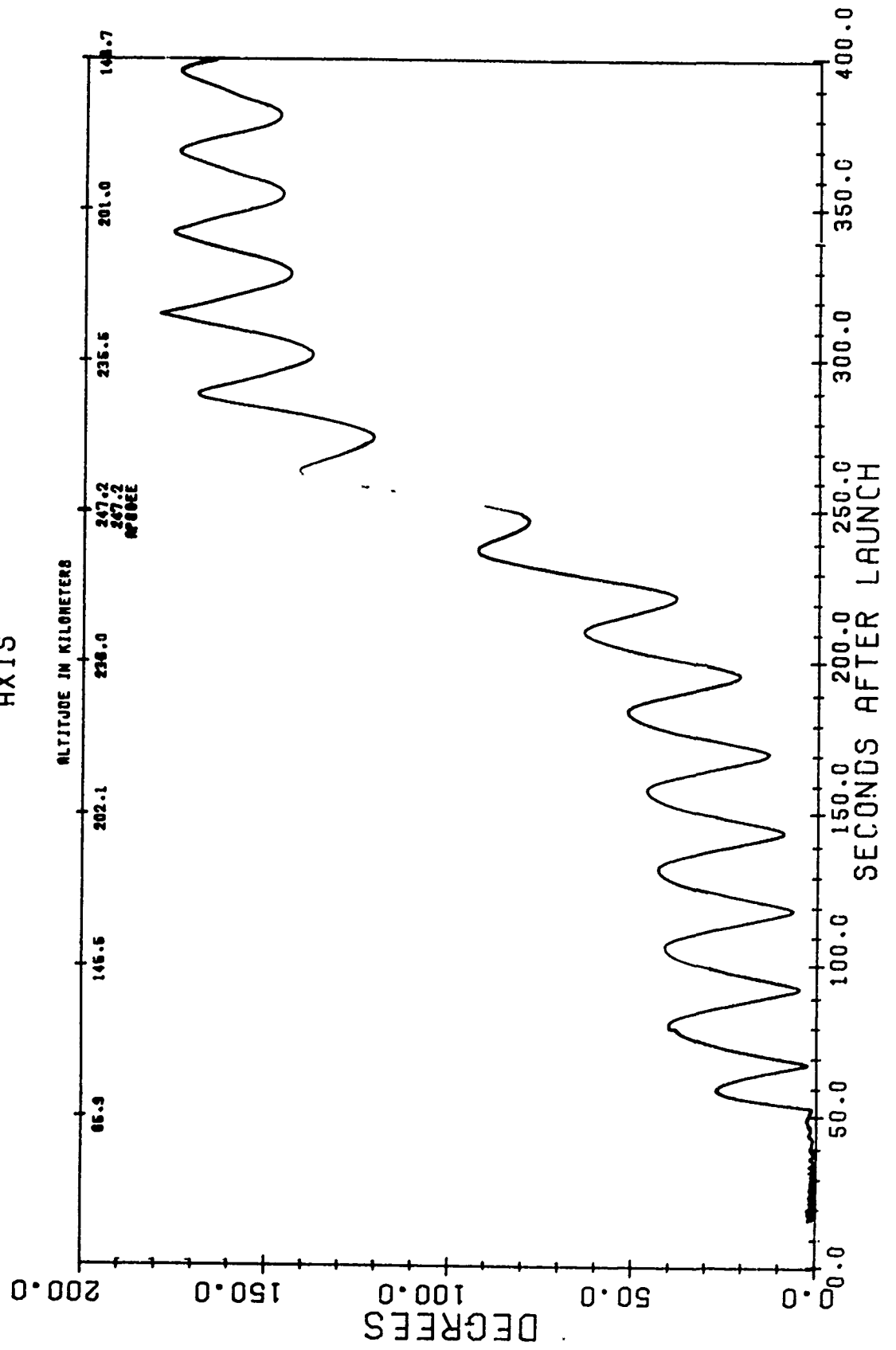


Figure 7

Figure 8

A09.210-2

ANGLE OF ATTACK

AXIS

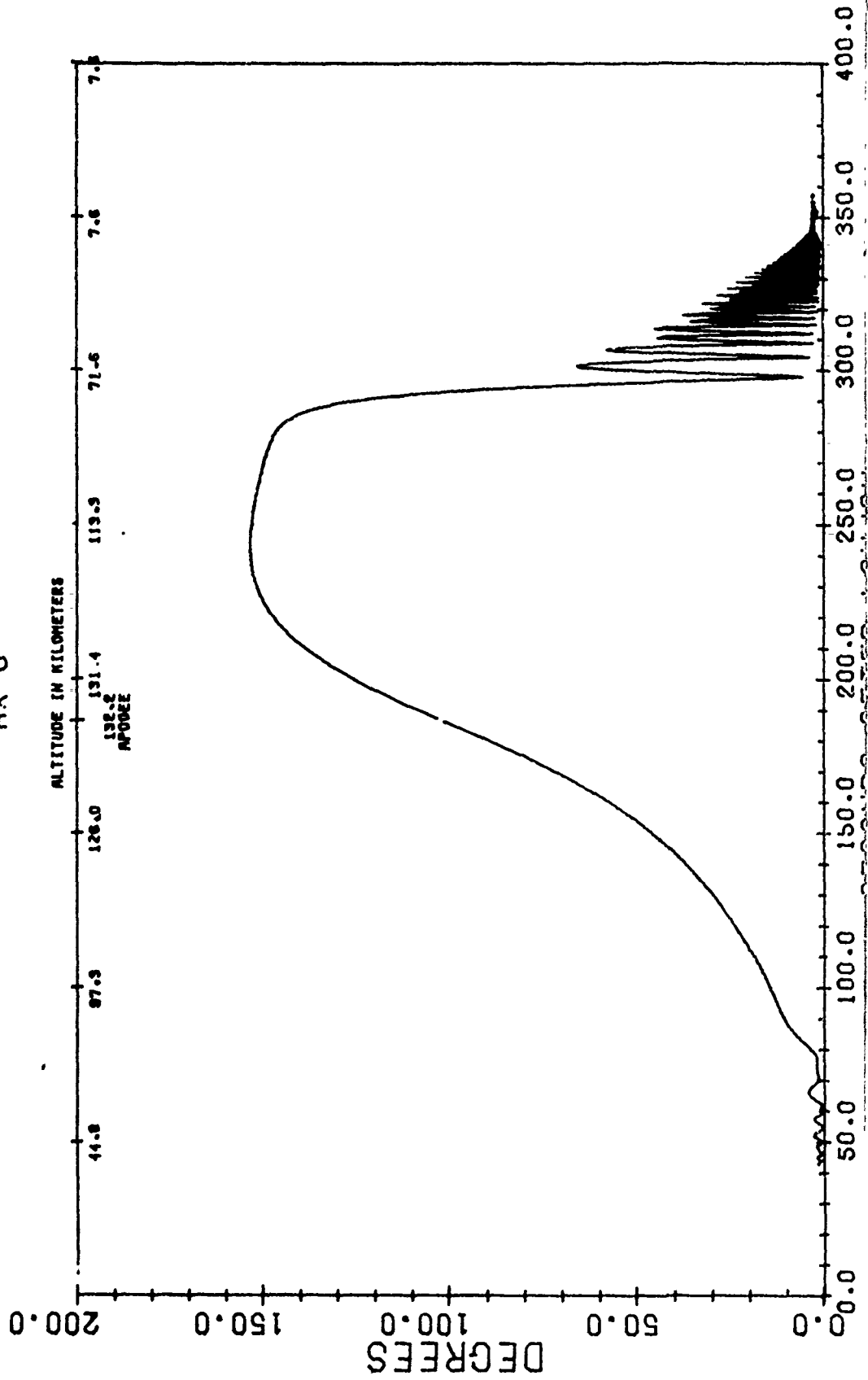


Figure 9

A09.210-1

ANGLE OF ATTACK

AXIS

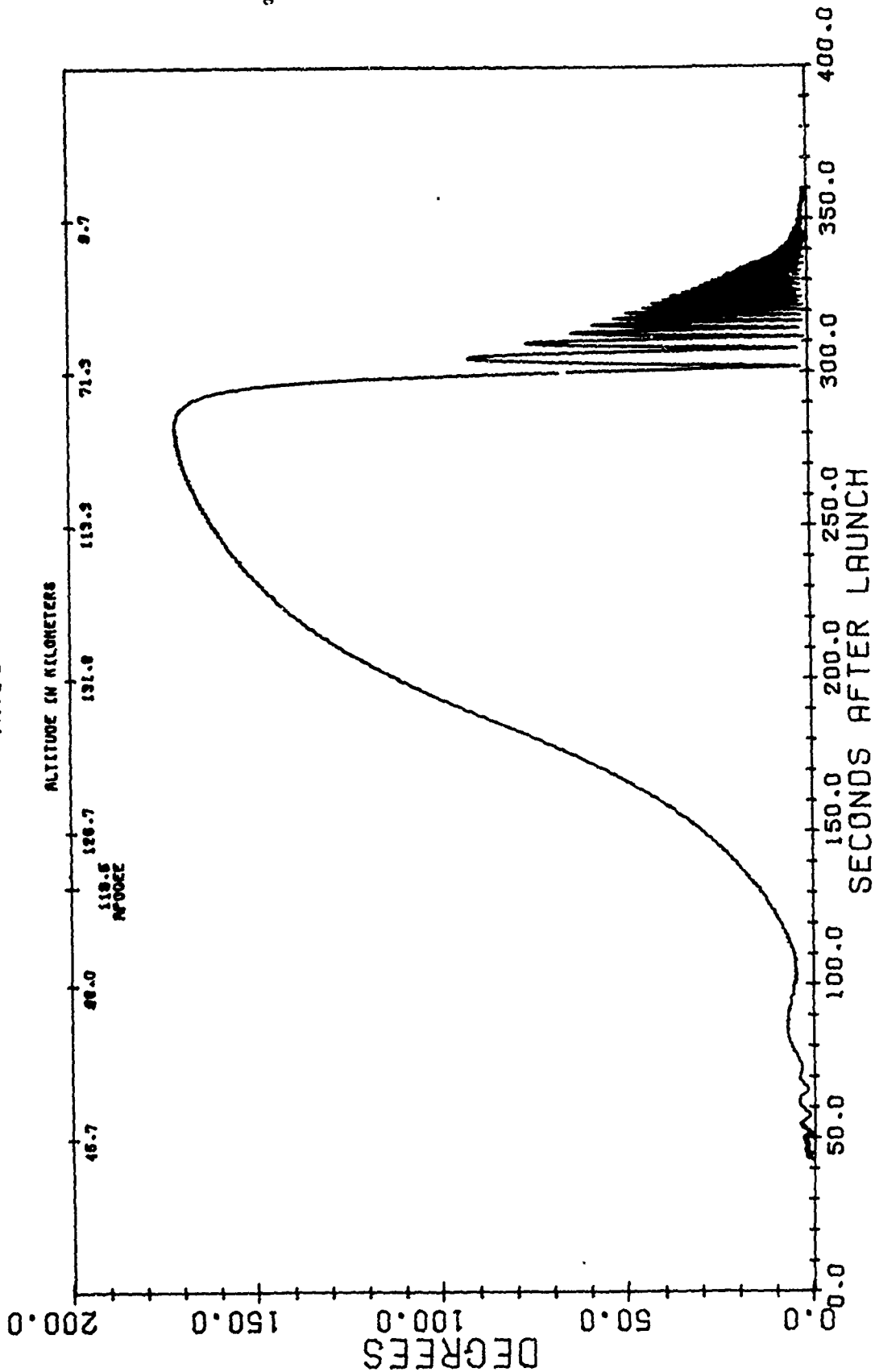


Figure 10

A17.110-1  
ANGLE OF ATTACK  
AXIS

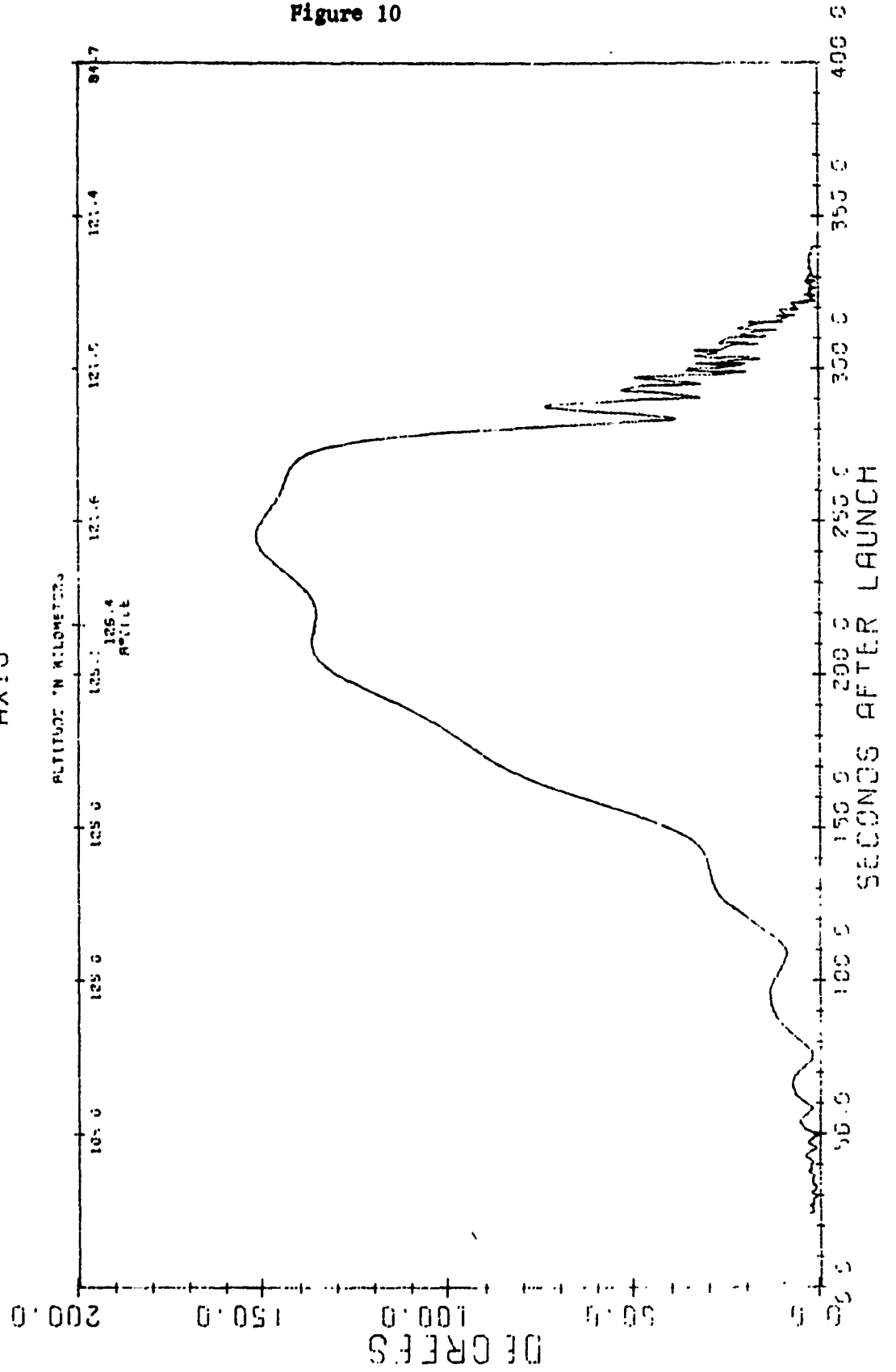
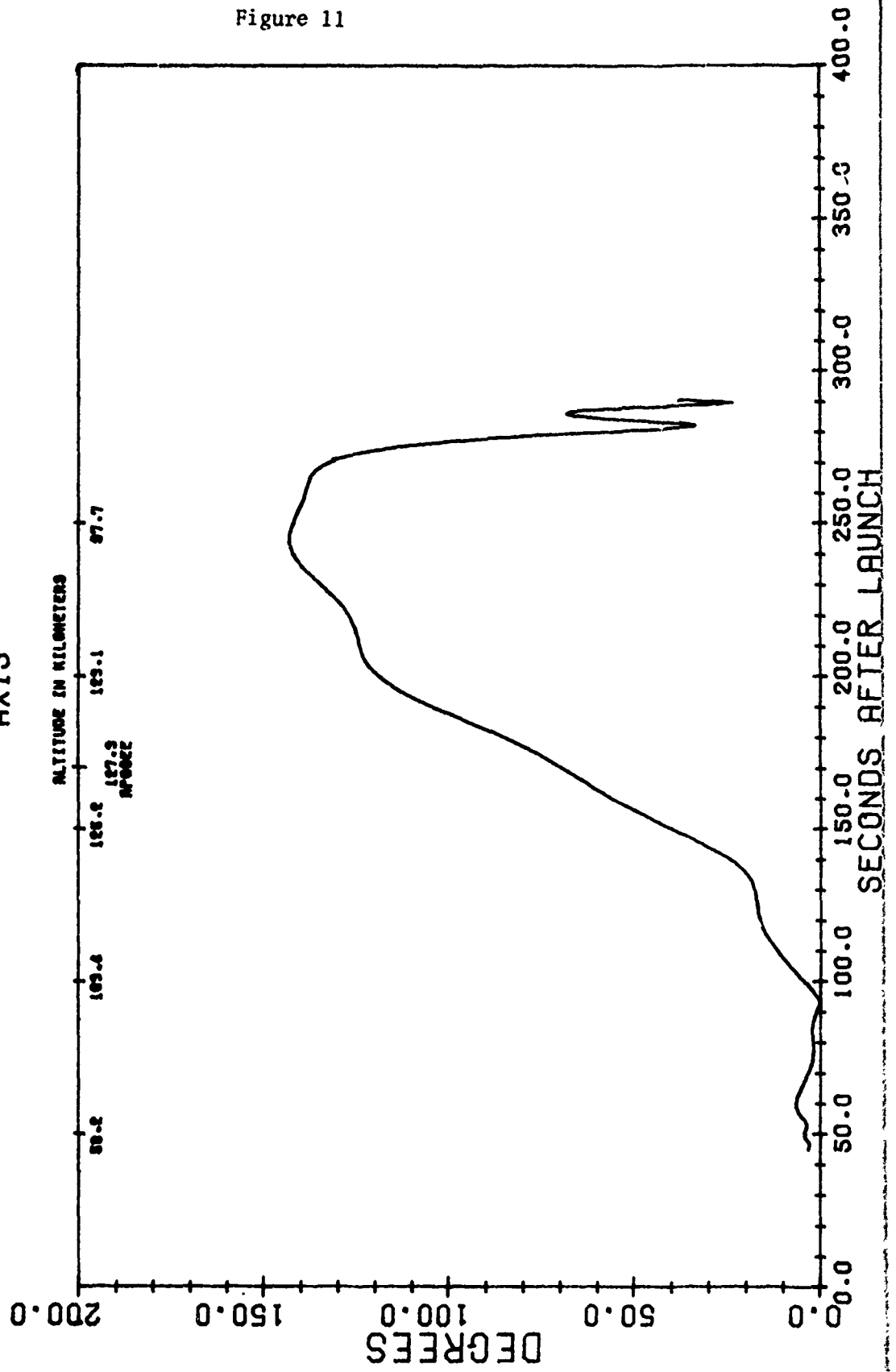


Figure 11

A17.110-2  
ANGLE OF ATTACK  
AXIS



A18.205-1

ANGLE OF ATTACK

AXIS

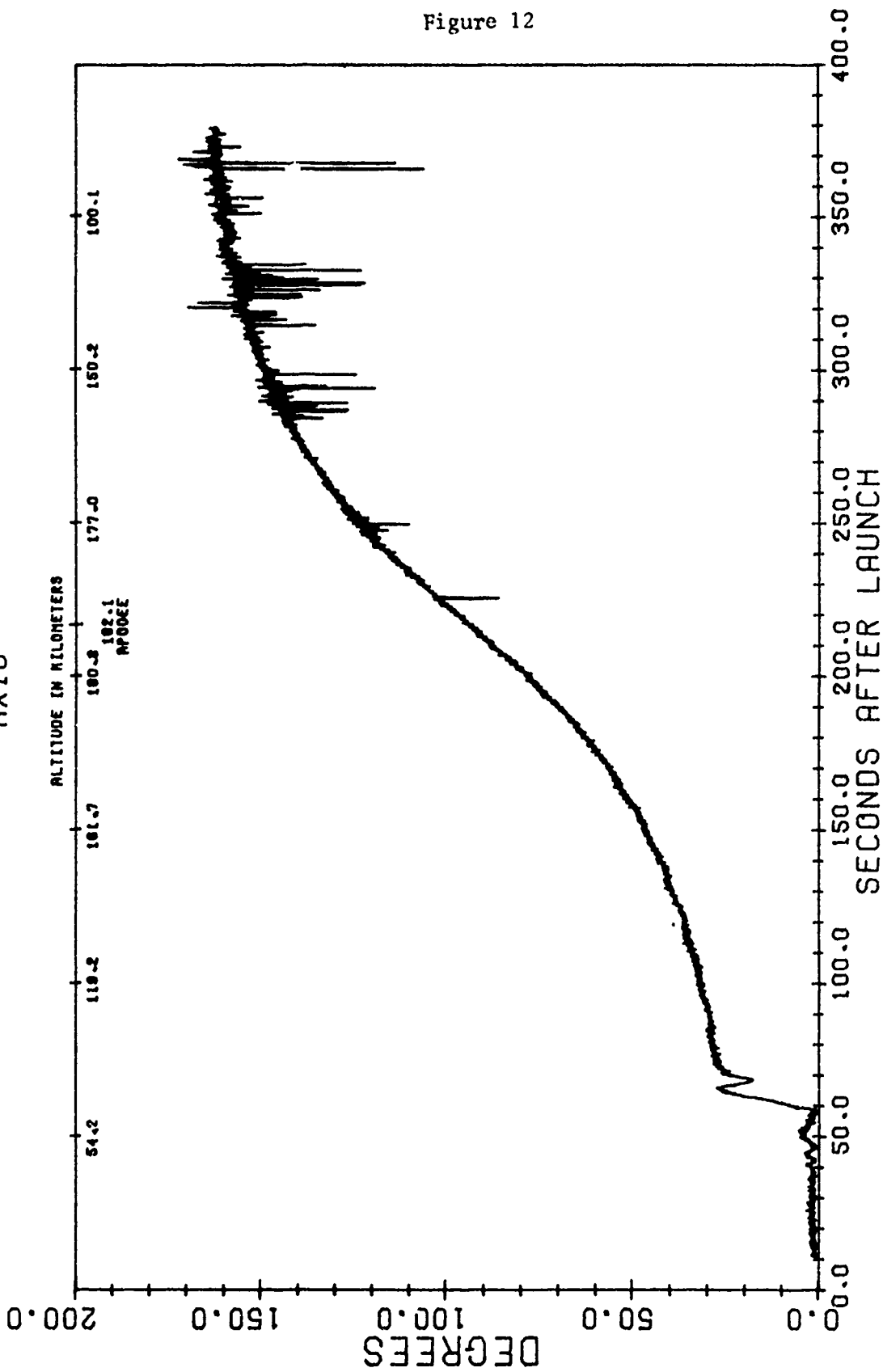


Figure 12

A18-205-1

ANGLE OF ATTACK

AXIS

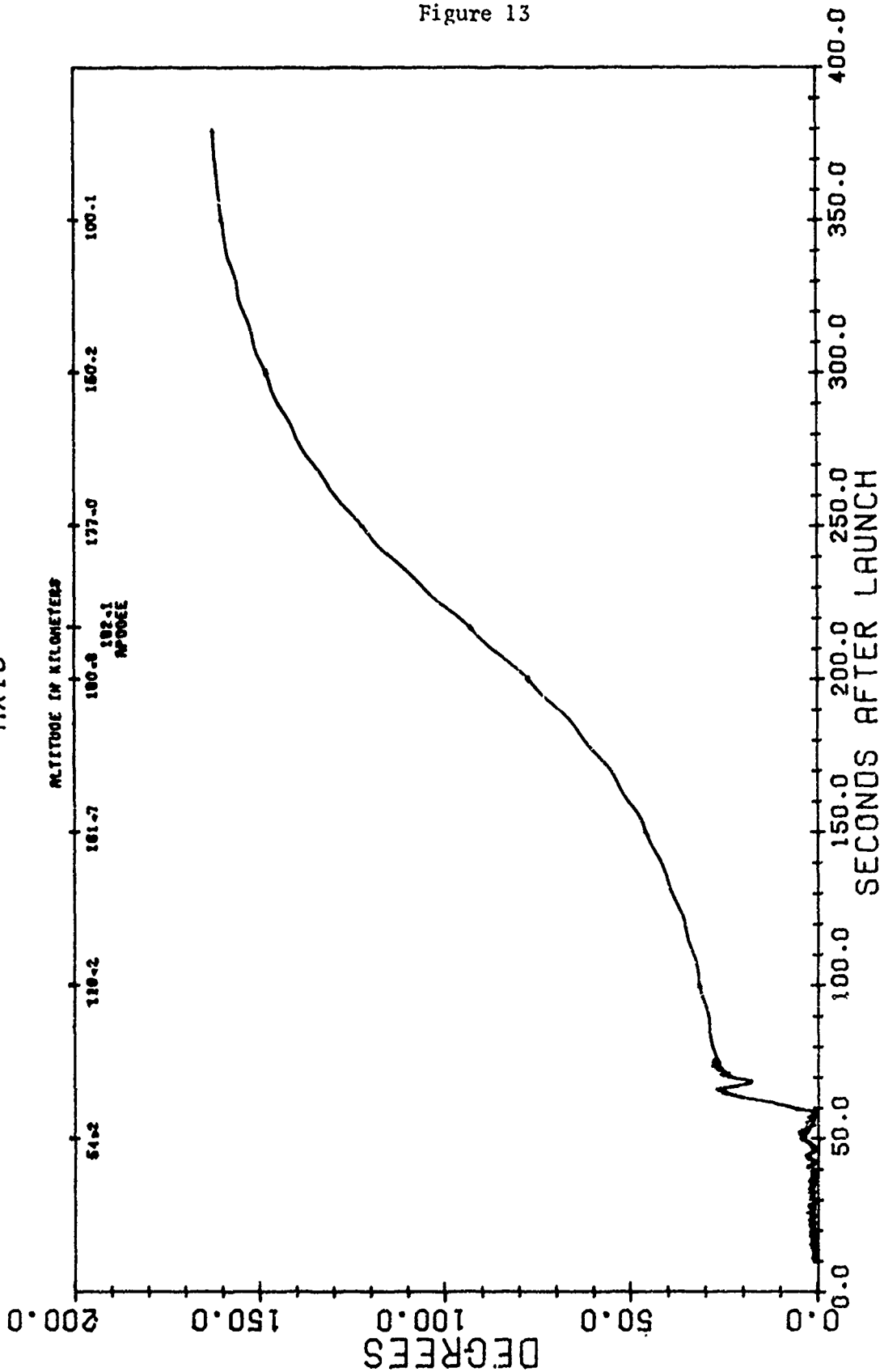


Figure 13

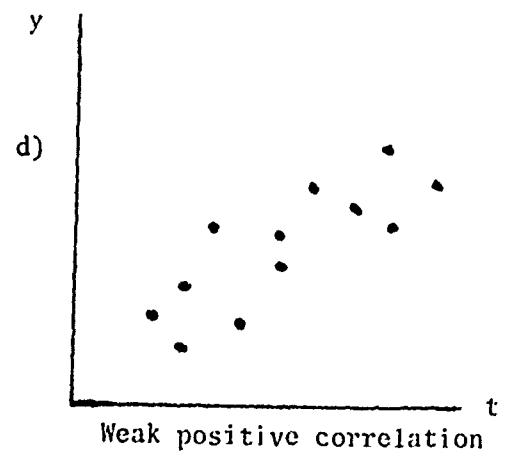
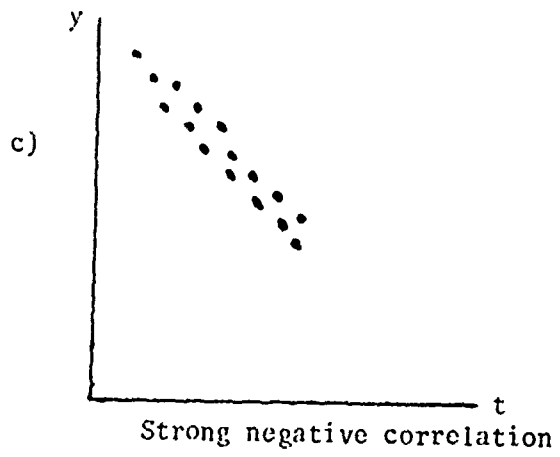
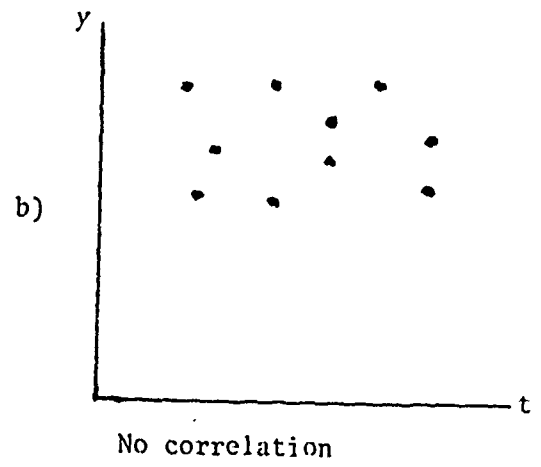
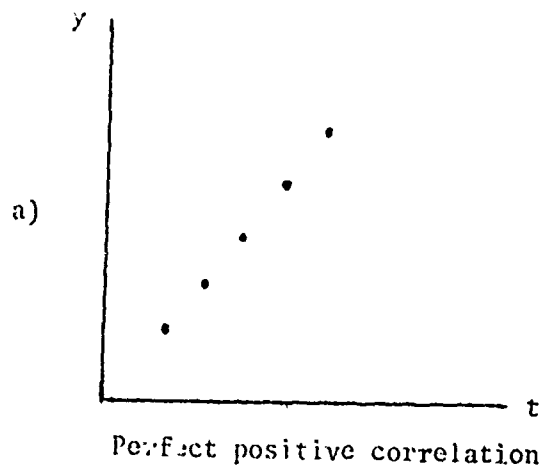


Figure 14

TYPICAL LINEAR CORRELATION STRENGTHS

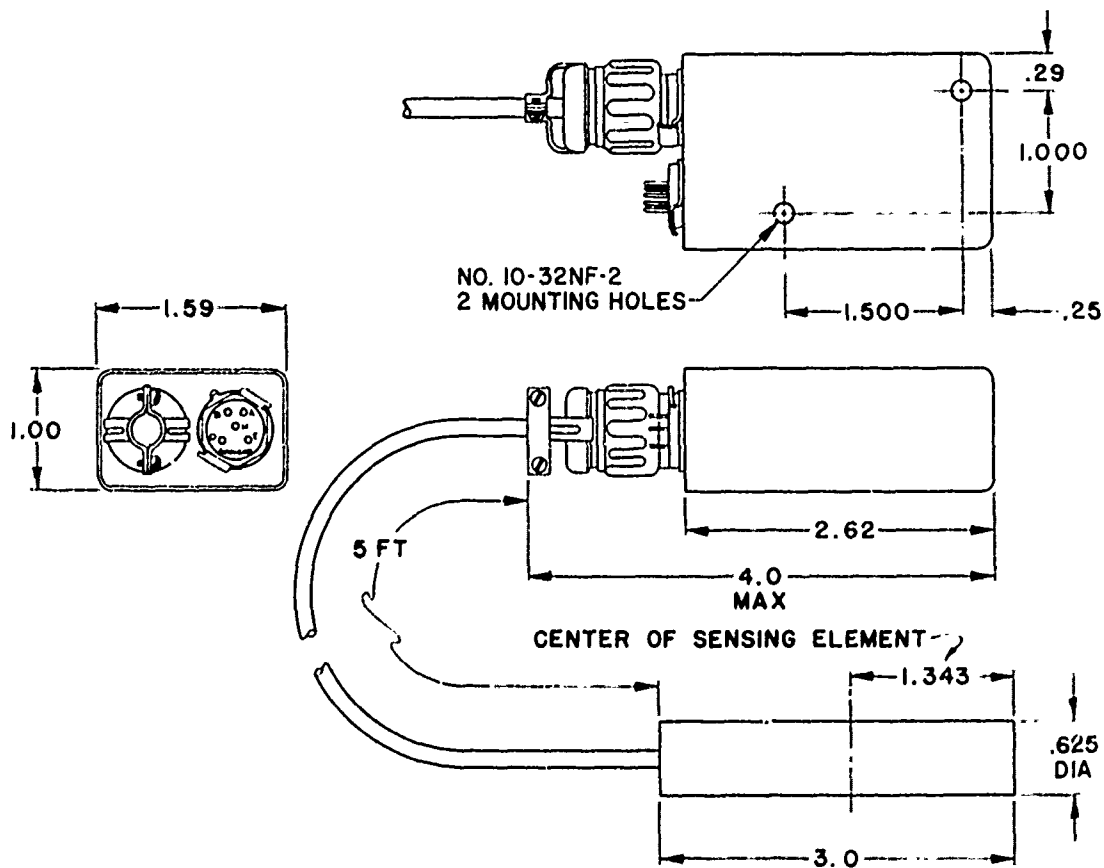


# RAM-5C SPECIFICATIONS

Figure 18

Input voltage: 24 to 32 volts dc  
 Input current: 11 milliamperes (typical)  
 Range of field: 0 to  $\pm 600$  millioersted  
 Sensitivity: .004 volts dc per millioersted  
 Stability of sensitivity:  $\pm 3\%$   
 DC output for zero field:  $2.40 \pm .02$  volts dc\*  
 Stability of output for zero field:  $\pm .025$  volts dc  
 Operating temperature range:  $165^\circ\text{F}$  to  $0^\circ\text{F}$  ( $\pm 185^\circ\text{F}$  to  $-50^\circ\text{F}$  with reduced accuracy)  
 Linearity:  $\pm 3\%$  of full scale  
 Frequency response: 195 Hz (typical)  
 Output impedance: less than  $20\text{ k}\Omega$   
 Output load (for factory calibration):  $100\text{ k}\Omega$   
 Length of sensor cable: 5 feet  
 Weight: 5 ounces

\*Standard units are biased as specified. An instrument, designated RAM-5C NB, is available with factory modification to provide 0-volt output for zero field.



SCHONSTEDT INSTRUMENT COMPANY  
 1775 WIEHLE AVENUE  
 RESTON, VIRGINIA 22070  
 Area Code 703 471-1050

Figure 19

CALIBRATION DATA

HELI FLUX<sup>®</sup>  
MAGNETIC ASPECT SENSOR  
TYPE RAM-5C

Field in Milligauss	Output Signal in Volts DC
600	<u>4.80</u>
550	<u>4.62</u>
500	<u>4.43</u>
450	<u>4.23</u>
400	<u>4.02</u>
350	<u>3.81</u>
300	<u>3.61</u>
250	<u>3.40</u>
200	<u>3.20</u>
150	<u>3.00</u>
100	<u>2.80</u>
50	<u>2.60</u>
0	<u>2.40</u>
-50	<u>2.21</u>
-100	<u>2.01</u>
-150	<u>1.81</u>
-200	<u>1.61</u>
-250	<u>1.41</u>
-300	<u>1.21</u>
-350	<u>1.00</u>
-400	<u>.79</u>
-450	<u>.58</u>
-500	<u>.38</u>
-550	<u>.19</u>
-600.	<u>+0.02</u>

(Bias Level)



Direction of Magnetic Field for Voltage Signals Above Bias Level

NOTE:

Calibration made with a 100k OHM resistor from signal output to negative terminal of battery source, and a 100k OHM resistor from bias output to negative terminal of battery source.

SCHONSTEDT INSTRUMENT COMPANY  
RESTON, VIRGINIA

Figure 20

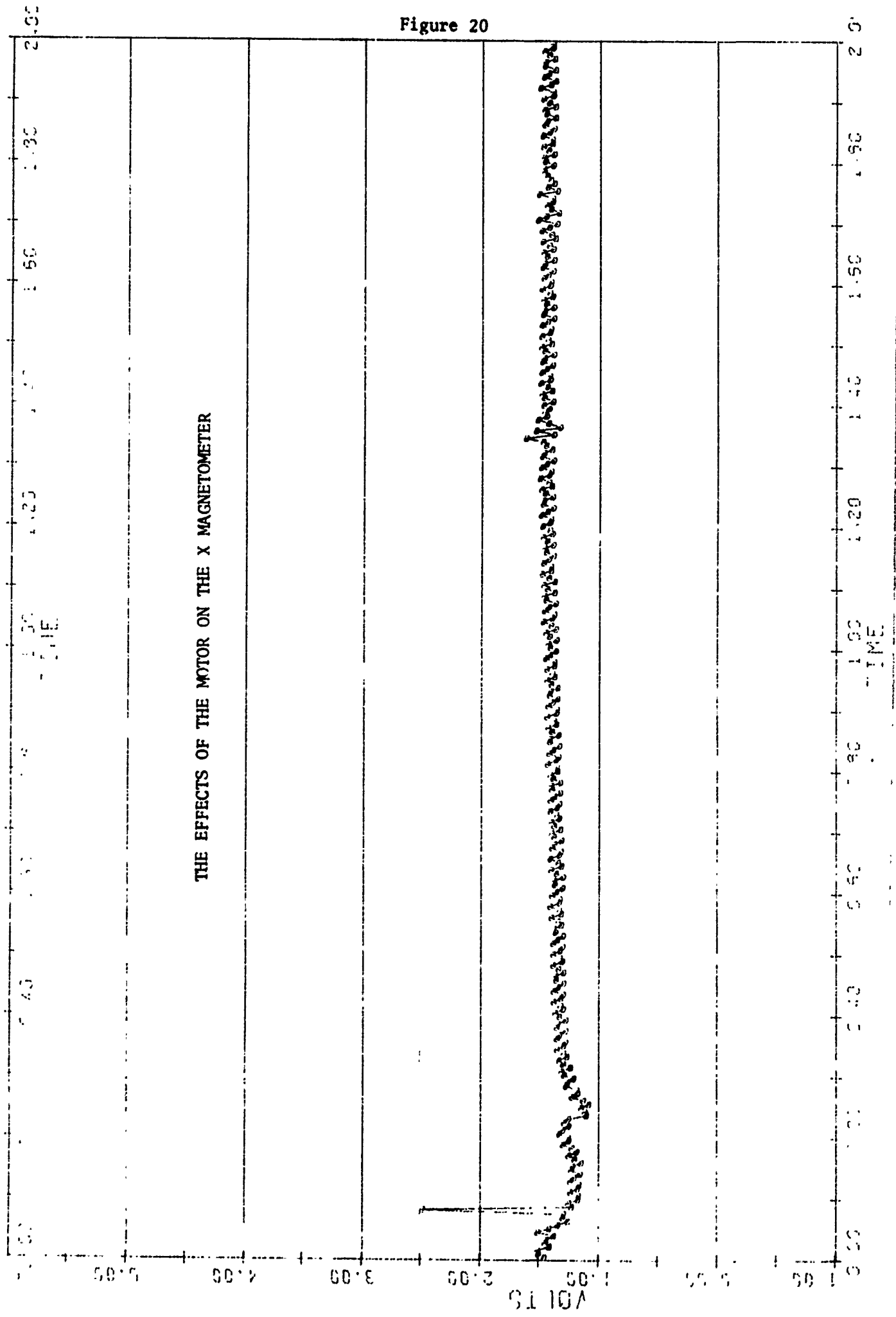


Figure 21

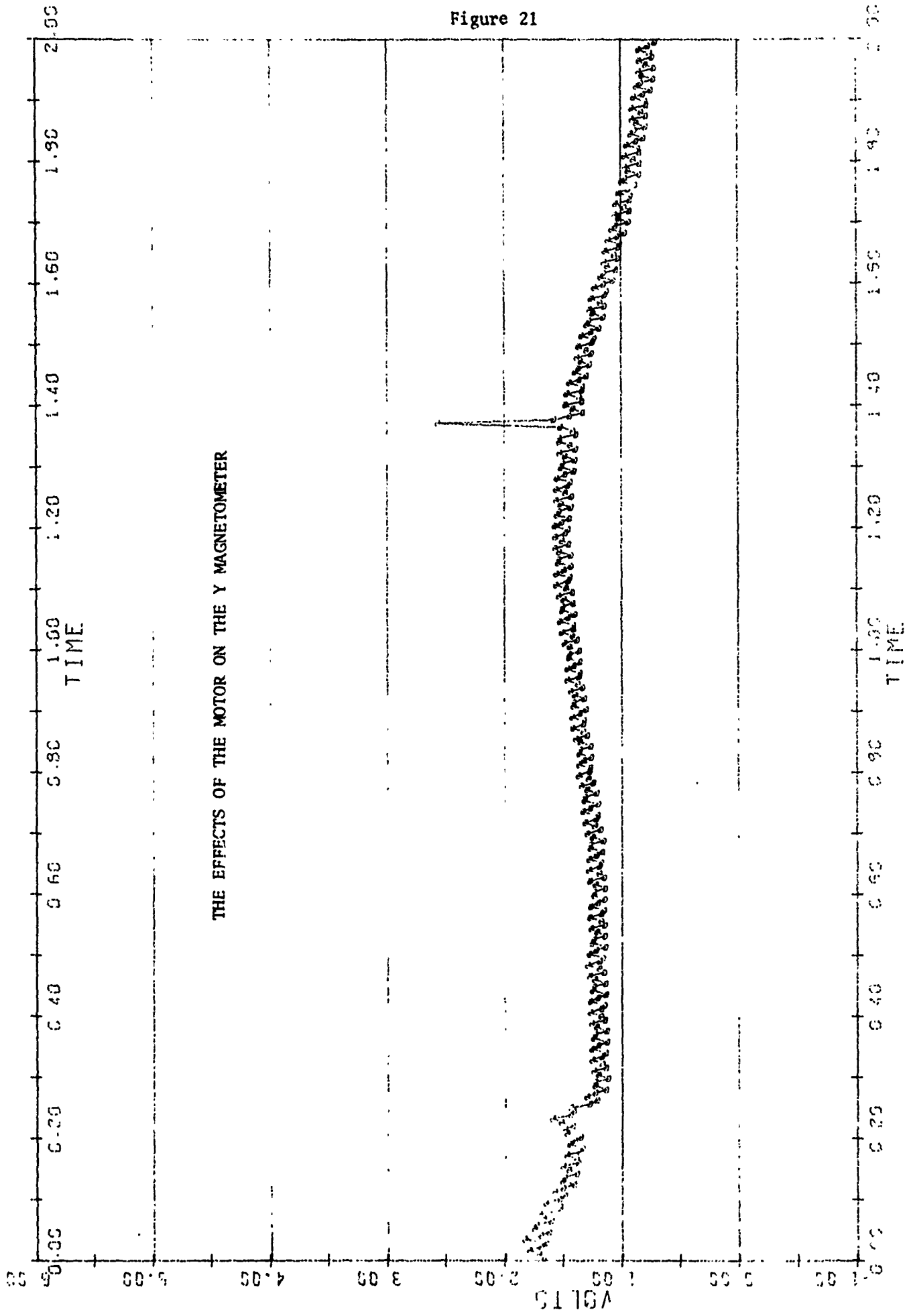
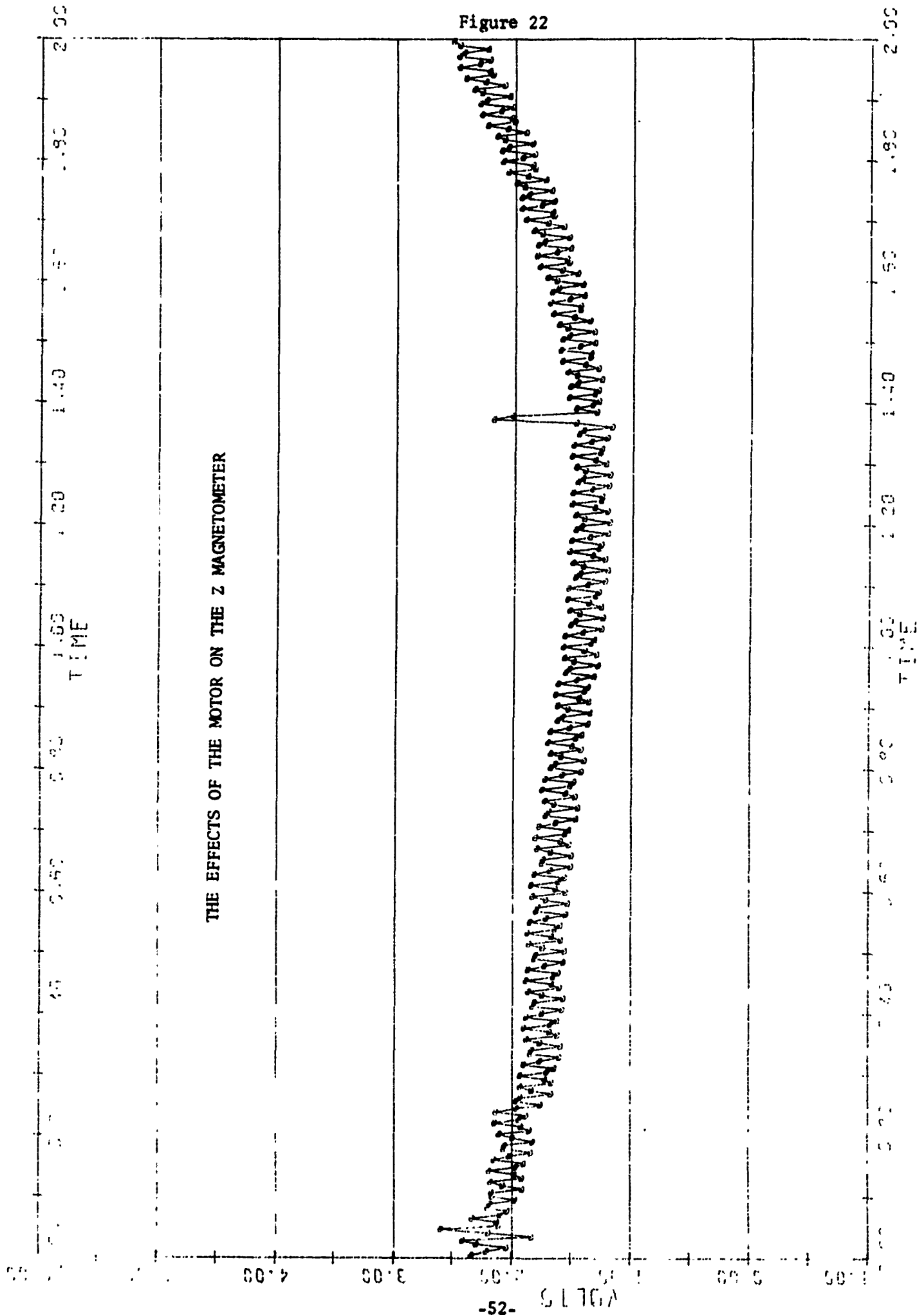


Figure 22



LSQMAG FLOWCHART

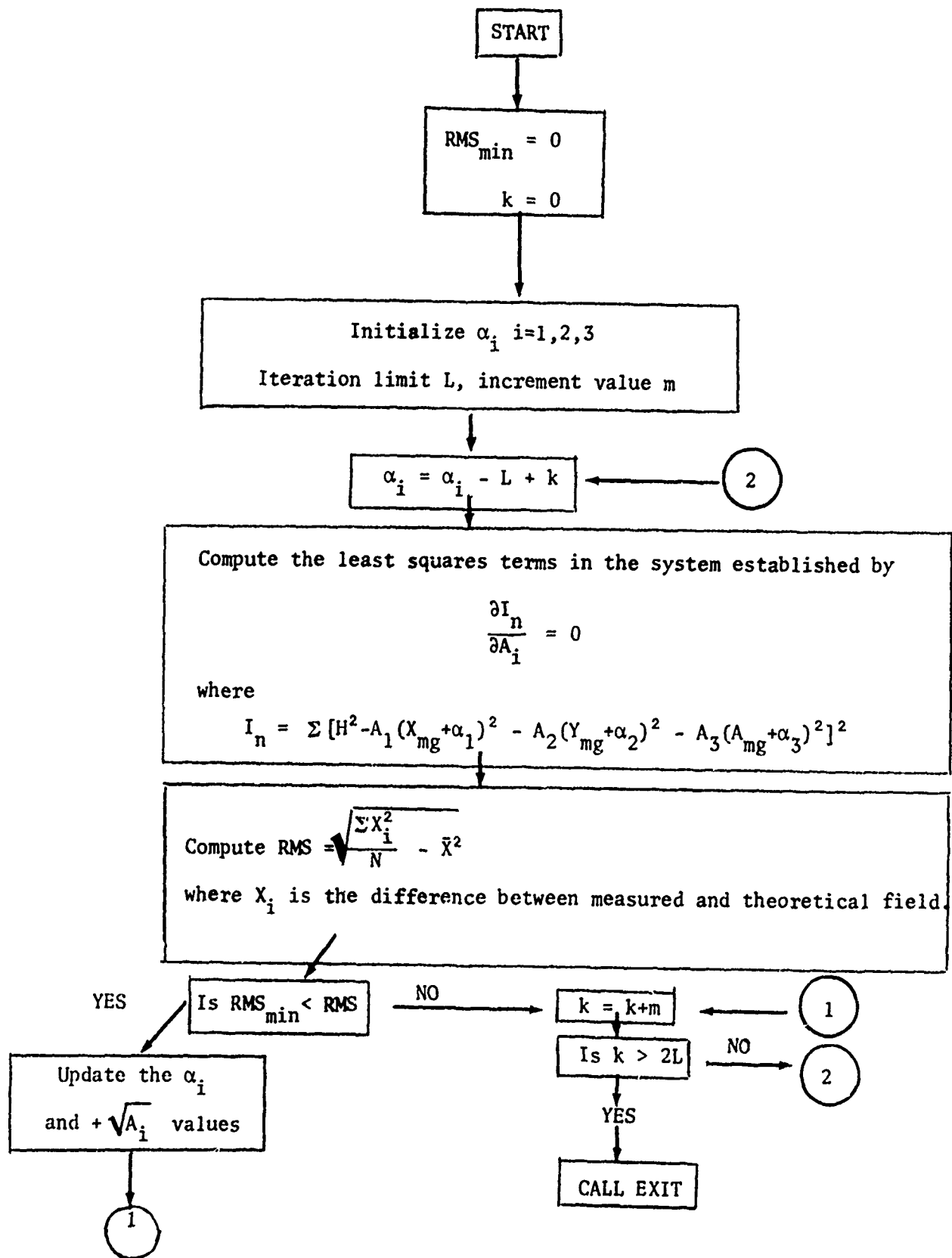
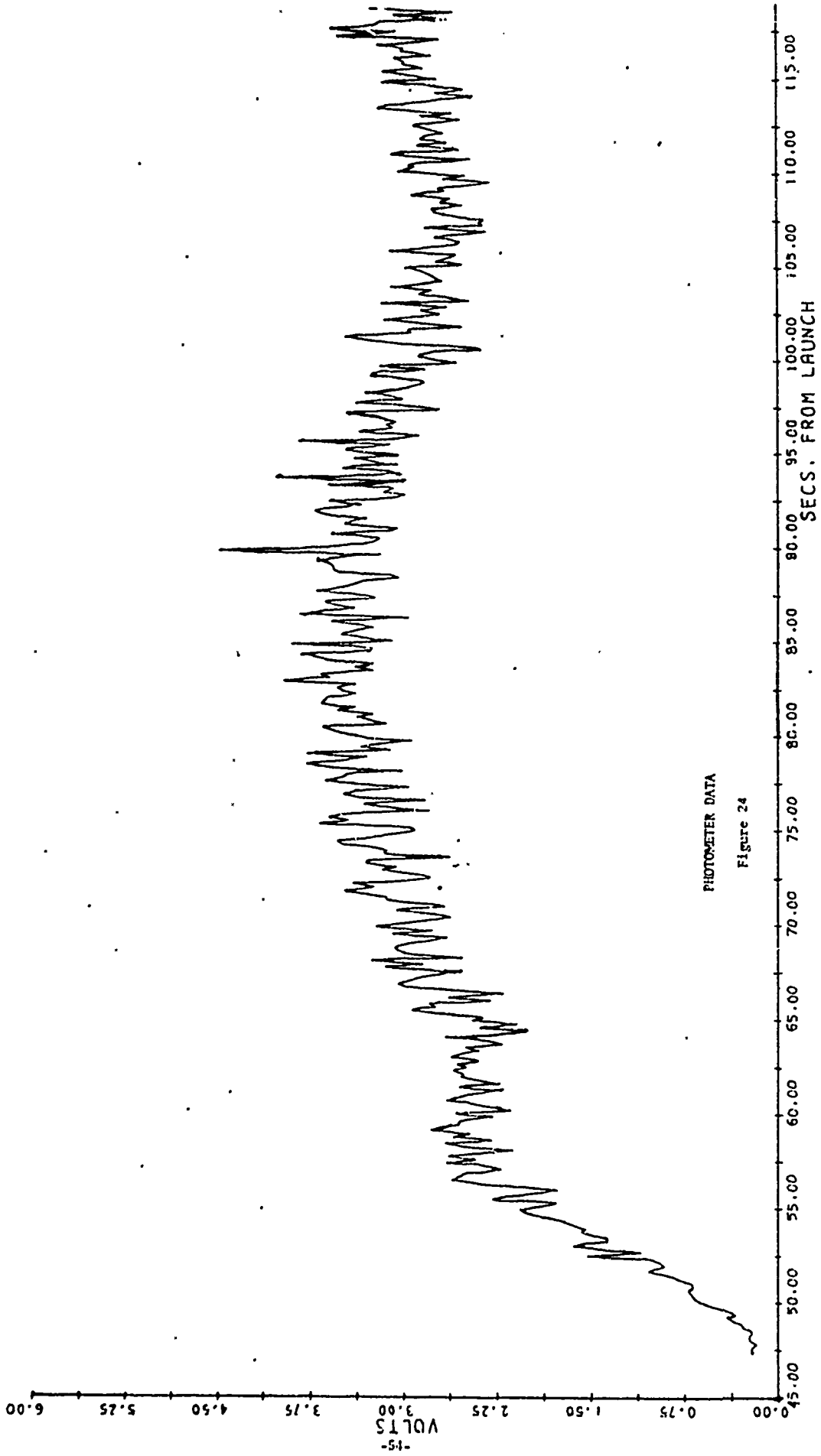


Figure 23



PHOTOMETER DATA

Figure 24

Figure 25

A03.208-1

ANGLE OF ATTACK

AXIS

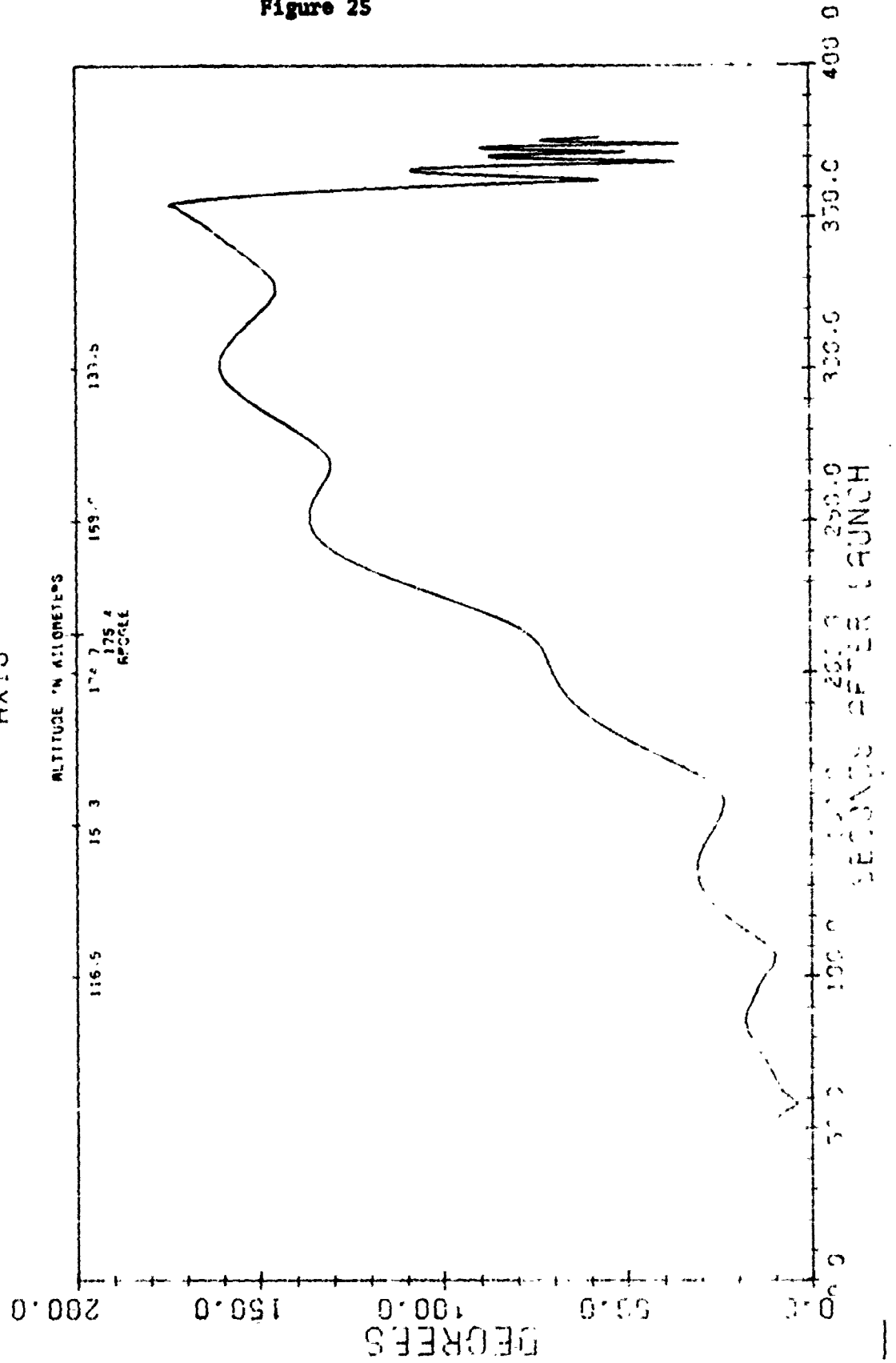


Figure 26

809-202-

LUNAR PITCH ANGLE

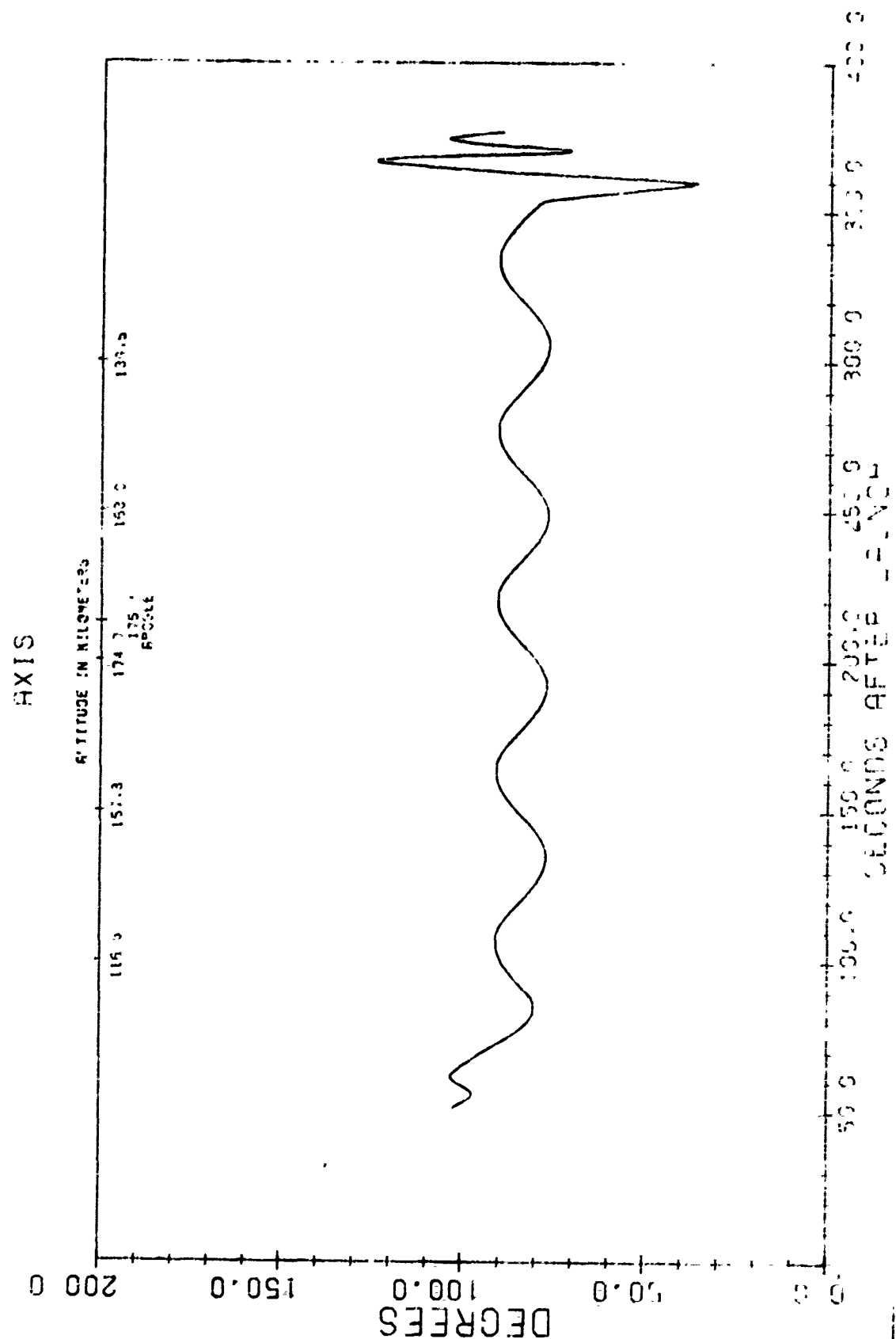
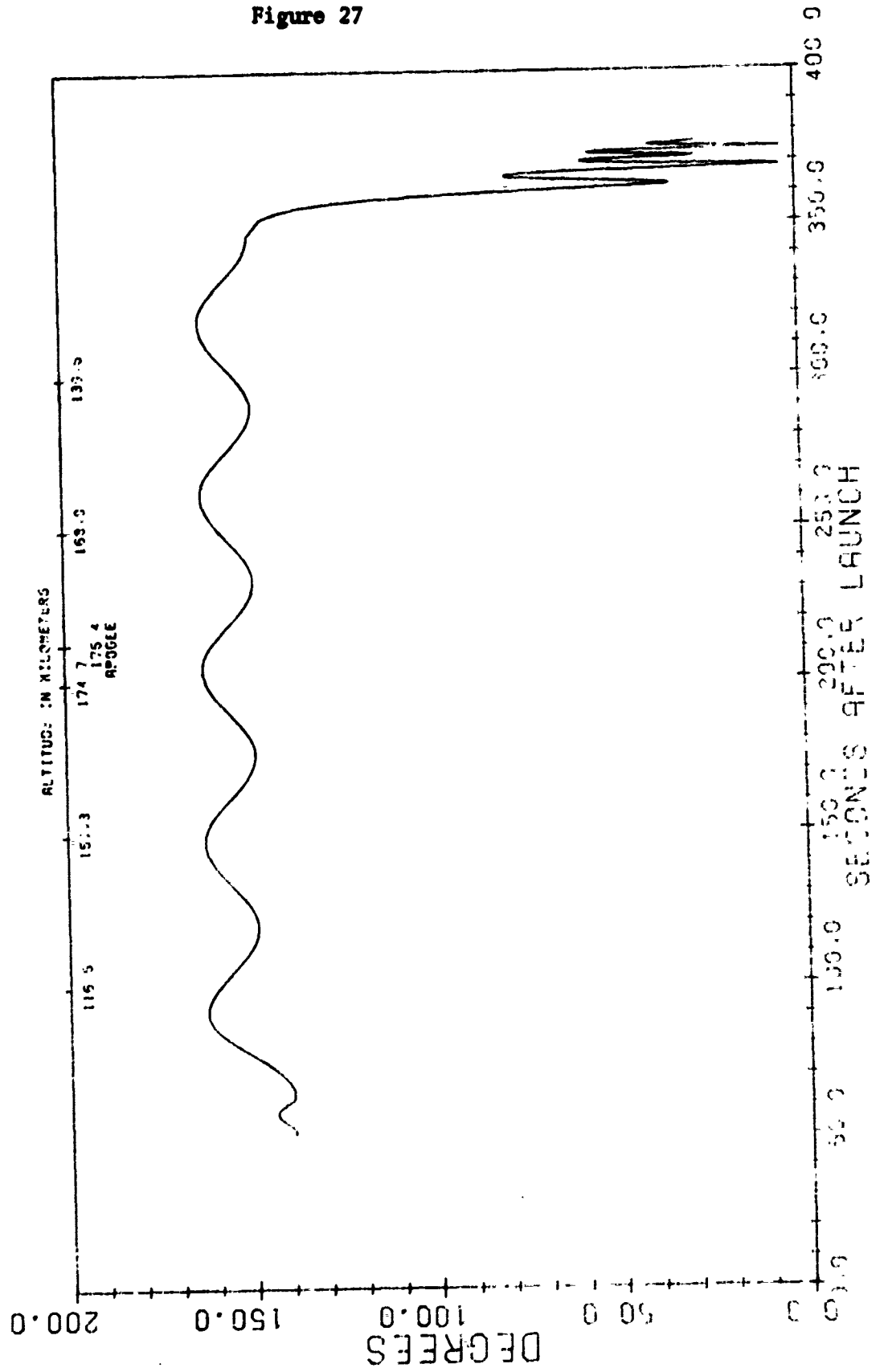


Figure 27

A03 209-1

MAGNETIC PITCH ANGLE

ROCKET AXIS



A09-209-1

# LUNAR PITCH ANGLE

MOON

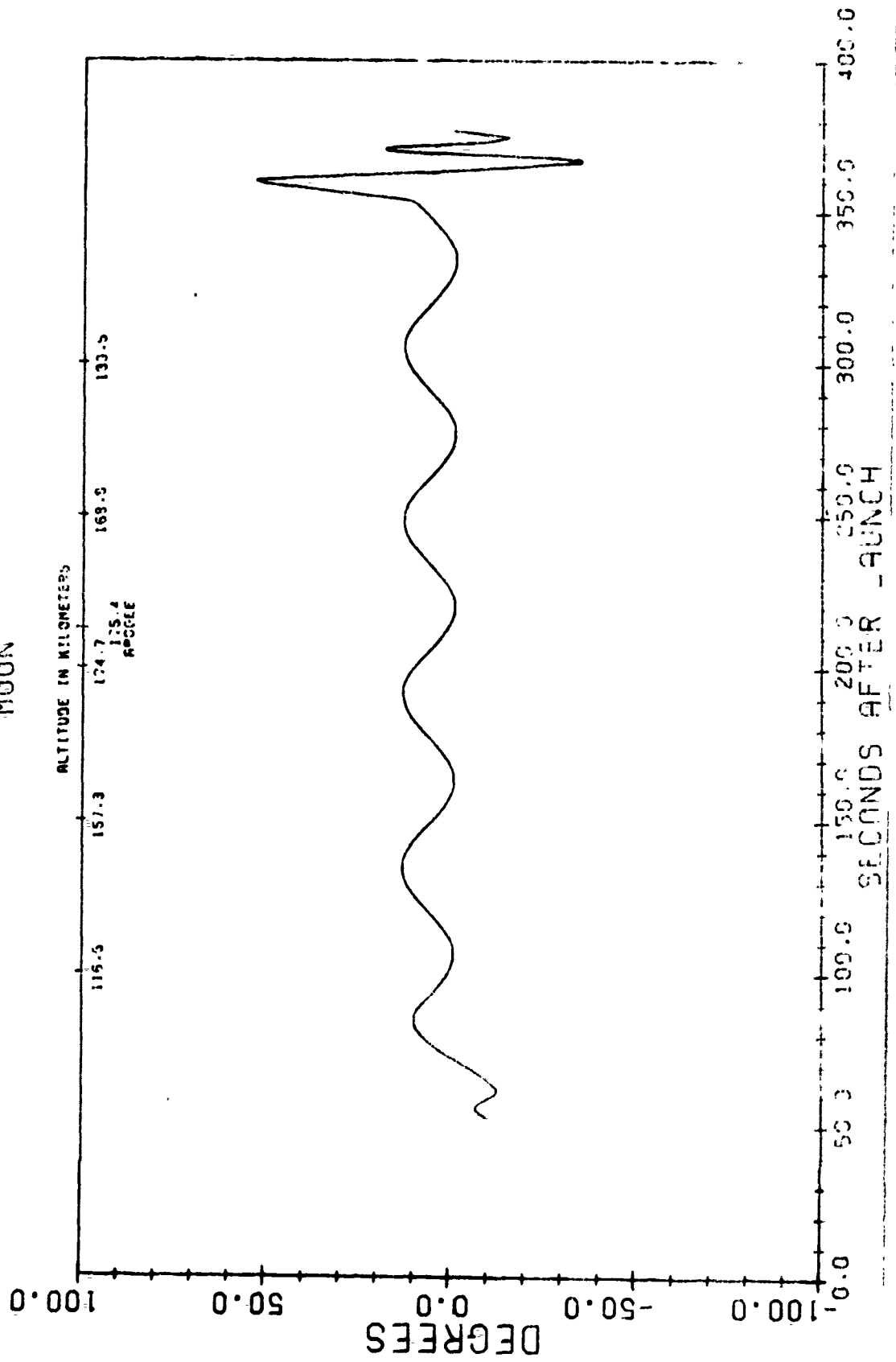


Figure 28

A09.209-1 LUNAR ANGULAR READOUTS

TIME (GMT)	ANGLE
11 hrs. 10 min. 18.02 sec.	+10°
11 hrs. 10 min. 18.2 sec	+ 5°
11 hrs. 10 min. 18.575 sec.	+ 0°
11 hrs. 10 min. 24.445 sec.	+ 5°
11 hrs. 10 min. 24.625 sec.	+10°
11 hrs. 10 min. 26.575 sec.	+10°
11 hrs. 10 min. 27.05 sec.	+ 5°
11 hrs. 10 min. 27.35 sec.	0°

Note: these outputs are all within ± 4° of the true angular value.

Figure 29

A09.209-1  
AXIAL MAGNETOMETER CORRECTED OUTPUT

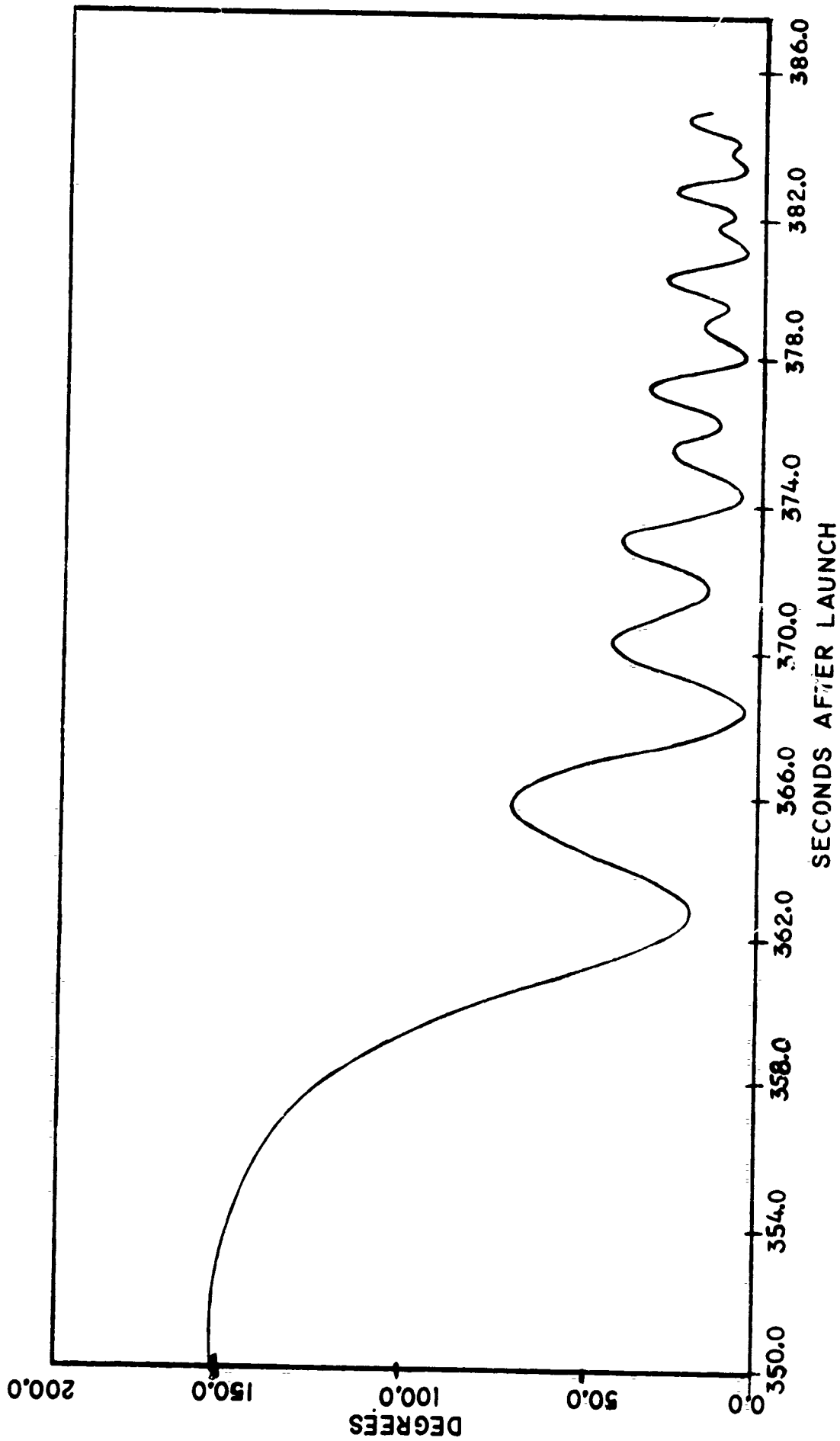


Figure 30

## REFERENCES

- [1] Judy A. Roxborough, Brian F. Sullivan, Rene J. Marcou, Marvin E. Stick, Kathleen M. Geezil, Procedures for the Determination of the Attitude of a Rocket from Gyroscopic Data, Boston College, Final Report for Contract Number F19628-70-C-0017 (United States Air Force, 1972).
- [2] Brian F. Sullivan, Marvin E. Stick, Rene J. Marcou, Techniques for Determining the Vehicle Attitude of Rocket AH7.886, Boston College, Scientific Report Number 1, prepared under Contract Number F19628-70-C-0017, (United States Air Force, 1972).
- [3] Rene J. Marcou, John A. Sandock, Brian F. Sullivan, Aspect of the Nike Cajun AB6.197 Fired 27 October 1964 from Fort Churchill Manitoba, Canada, Boston College, Scientific Report No. 2, prepared under Contract Number AF19628-4178, (United States Air Force, 1965).
- [4] Rene J. Marcou, Brian F. Sullivan, Aspect of a Rocket from Magnetometer Data, Boston College, Final Report, for Contract AF19628-4178, (United States Air Force, 1967).
- [5] Robert A. Crovelli, Principles of Statistics and Probability, Prindle, Weber and Schmidt, Inc., Boston, Mass., 1973.

## BIBLIOGRAPHY

Kij, Arthur F., Fundamentals of Electricity and Magnetism. McGraw-Hill, N.Y., 1962.

Sears, Francis W., Electricity and Magnetism, Addison-Wesley, Reading, Mass. 1951.

Young, Hugh D., Statistical Treatment of Experimental Data, McGraw-Hill, Book Co., Inc., 1962.

### ACKNOWLEDGMENTS

The authors wish to acknowledge their debt to the many people of the Space Data Analysis Laboratory of Boston College who have supported the effort summarized in this report. First, we wish to thank Mr. Leo F. Power, Jr., the Director of the Laboratory for his continual supervision and recommendations during this rocket attitude program. The major bulk of the software assistance was ably provided by Mr. Paul C. Fioretti and Ms. Linda Gosselin, assisted by Mr. Owen Marr. Mr. Raymond Blanchfield and Ms. Geraldine O'Brien also contributed to this effort. We also wish to thank Mr. Dennis E. Delorey, Mr. Joseph E. Martine, Mr. Paul N. Pruneau, and Ms. Carol I. Foley for their liberal advice and assistance in solving many of the programming difficulties. Special thanks are also due to Mr. Vincent Cahalane who lent his technical writing skills not only to the report but also during the entire reporting period. We also wish to thank Ms. Arnetis Akre for her patient and careful preparation of the manuscript.

We wish to express our sincere appreciation to Mr. Robert E. McInerney of AFCRL for his guidance in the execution of the rocket attitude determination system.